

1 2 9 0



UNIVERSIDADE DE
COIMBRA

José Diogo Coutinho de Carvalho Casca

IMPACT OF POSITION ERRORS ON
POSITION-ASSISTED DISTRIBUTED
BEAMFORMING IN WIRELESS SENSOR
NETWORKS

Dissertation in the context of the Master in Electrical and Computer Engineering, Specialization in Telecommunications, Subspecialization in Wireless and Optical Communications, supervised by Prof. Dr. Marco Alexandre Cravo Gomes and Prof. Dr. Vítor Manuel Mendes da Silva and presented to the Faculty of Sciences and Technology, Department of Electrical and Computer Engineering.

July 2024



FCTUC FACULDADE DE CIÊNCIAS
E TECNOLOGIA
UNIVERSIDADE DE COIMBRA

Impact of Position Errors on Position-Assisted Distributed Beamforming in Wireless Sensor Networks

José Diogo Coutinho de Carvalho Casca

Coimbra, July 2024



Impact of Position Errors on Position-Assisted Distributed Beamforming in Wireless Sensor Networks

Supervisor:

Prof. Doutor Marco Alexandre Cravo Gomes

Co-Supervisor:

Prof. Doutor Vitor Manuel Mendes da Silva

Prof. Doutor Rui Miguel Henriques Dias Morgado Dinis

Jury:

Prof. Doutora Maria do Carmo Raposo de Medeiros

Prof. Doutora Rita Cristina Girão Coelho da Silva

Prof. Doutor Marco Alexandre Cravo Gomes

Dissertation submitted in partial fulfillment for the degree of Master of Science in
Electrical and Computer Engineering.

Coimbra, July 2024

Agradecimentos

E com esta dissertação, cinco anos de curso passaram. Não apenas cinco anos, mas cinco anos repletos de histórias, novas amizades e lições de vida, e com alguns copos aqui e ali, mas poucos. E para que tudo isto fosse possível, há uma lista de pessoas a quem tenho de agradecer.

Primeiramente, gostava de agradecer aos meus pais pelo apoio e esforço para me proporcionar a vida académica desejada por muitos, por me chamarem à atenção quando me desleixava nos estudos e por me mostrarem que era capaz de fazer cada vez mais. À minha mãe, que mesmo longe ou a fazer milhares de quilometros por mês arranjava sempre tempo para que nada me faltasse e ao meu pai que me mostrou que os anos de douturamento lhe trouxeram muita experiência sobre como pesquisar artigos e escrever um bom documento *Piada sobre para o ano é que o douturamento acaba*. Não menos importantes, um obrigado aos meus irmãos por fazerem parecer que sou o estudante mais aplicado dentre os filhos e aos avós, madrinha e padrinho por estarem presentes ao longo do meu crescimento.

Em seguida, gostava de agradecer ao professor Marco pelo apoio nesta dissertação e que, apesar de um laboratório cheio de estudantes em mestrado e doutoramento, sempre consegui ajudar e guiar-me quando era mais necessário. Um obrigado também aos professores Vitor e Rui pelas ideias dadas e apoio prestado, sugestões e pela ajuda prestada durante a realização desta dissertação. Junto do apoio dos professores que me seguiram de perto, um obrigado também ao Instituto de Telecomunicações (IT) Coimbra pelo acesso a tudo o que precisei para completar este trabalho. Agradecer também o apoio de todos os professores presentes durante o meu percurso académico e a introdução feita a este mestrado que tanto me diz.

Ao NEEEC/AAC, e a todos que lá estiveram nos mandatos dos quais fiz parte, um obrigado pois, se sou quem sou hoje, é graças a tudo onde me pude envolver devido a esta bonita casa. E claro um especial obrigado ao Executivo. Diogo Flórido, André Neto e José Dias, 23/24 foi um ano complicado, até porque provavelmente já teria acabado a dissertação há uns meses se não fosse esta dor de cabeça, mas não seria o mesmo sem vocês e aquelas

primeiras reuniões no Café Reis.

E como nunca estamos sozinhos não me podia esquecer do círculo de amigos. À Flávia que, para além de amiga, virou uma companheira que passa quase tanto tempo no laboratório como eu e que bastante companhia me faz naquelas idas ao Mc para um gelado ao fim do dia. À "Família" de praxe, Kika, Catarina e Patrícia por estes longos anos de amizade criada por uma simples ida para uma filarmónica da terrinha. À Bárbara um obrigado pelo retorno de uma pessoa fofoqueira para atualizar as histórias da pequena vila da Lousã. Ao meu padrinho Lins por ser um exemplo de como escrever relatórios e estudar para frequências. Ao maior grupo de pessoas queimadas da cabeça, com lugar de encontro TrapHouse, pelas saídas por Coimbra ou simplesmente uma noitada de MarioKart ou Buzz. E por fim, a um amigo muito especial que me marcou, Magano, um obrigado e foi um prazer conhecer-te mas agora que vais para informática temos de rever esta amizadade.

Por fim, e para não me escapar ninguém, um obrigado à Orquestra Ligeira das Gândaras e à Sociedade Filarmónica Lousanense que me abriram o caminho para que as caminhadas de um músico amador fossem possíveis. À TAUC, pelas oportunidades de concertos e ensaios de pedir por mais. A todos os que passaram pela Secção de Boxe e Lutas da AAC, principalmente ao Pinypon, por me mostrarem que um desporto individual pode unir tanto as pessoas quanto um desporto coletivo.

Para as pessoas que leram até aqui, um obrigado pela paciência e se me esqueci de alguém, acrescentar em baixo:

Funding Acknowledgement

Este trabalho é financiado por fundos nacionais através da FCT - Fundação para a Ciência e a Tecnologia, I.P., no âmbito do projeto 10.54499/UIDB/50008/2020, com o identificador DOI, <https://doi.org/10.54499/UIDB/50008/2020>

This work was supported by FCT - Fundação para a Ciência e Tecnologia, I.P. by project reference 10.54499/UIDB/50008/2020, and DOI identifier

<https://doi.org/10.54499/UIDB/50008/2020>

Resumo

Ao longo dos anos, o interesse pelas redes de sensores sem fios, vulgo *Wireless System Networks* (WSNs), cresceu significativamente devido às suas diversas aplicações, como monitorização meteorológica, controlo de temperatura, medição de humidade e avaliação da qualidade do ar. As WSNs baseiam-se em numerosos nós de energia muito baixa, cada um servindo como sensor e constituindo a principal fonte de comunicação. O número considerável de sensores e o alcance limitado da capacidade de transmissão desses nós representam um desafio para as WSNs na recolha de dados dos sensores. De facto, as WSNs podem ser consideradas um sistema multi-utilizador Multiple Input Multiple Output (MIMO) distribuído.

Beamforming, que são técnicas de processamento de sinal que concentram a potência de transmissão numa direção específica, tem sido explorado tem vindo a ser explorado o uso de técnicas de confinamento feixe, i.e. para lidar com limitações de alcance em WSNs. No entanto, a aplicação bem-sucedida das técnicas de *beamforming* convencionais, depende do conhecimento preciso da localização dos sensores, constituindo um desafio em sistemas MIMO distribuídos como as WSNs, isto porque, informações imprecisas sobre a localização do sensor podem degradar significativamente a eficácia do *beamforming*.

Este trabalho foca-se no estudo do impacto de erros de posição em WSNs no desempenho das técnicas de enquanto utiliza *distributed beamforming* aplicados às WSNs. Várias topologias de rede e técnicas serão avaliadas para estudar o comportamento dos sistemas em diferentes cenários.

Palavra-Chave: Wireless System Networks, Multiple Input Multiple Output, Distributed Beamforming, Communications & Sensing, Processamento de Sinal

Abstract

The interest in Wireless Sensor Networks (WSNs) has grown significantly over the years due to their diverse applications, such as weather monitoring, temperature control, humidity measurement, and air quality assessment. WSNs rely on numerous very low-energy nodes, each serving as a sensor, constituting the primary communication source. The considerable number of sensors and limited transmitting capacity range of these nodes present a challenge for WSNs when collecting data from the sensors. In fact, WSNs can be considered a distributed multi-user Multiple Input Multiple Output (MIMO) system.

Beamforming is a signal processing technique that focuses transmission in a particular direction and has been explored to address range limitations in Wireless Sensor Networks (WSNs). However, the successful application of conventional beamforming, which relies on precise knowledge of sensor locations, remains a challenge in distributed MIMO systems like WSNs. This is because inaccurate sensor localization information can significantly degrade beamforming's effectiveness.

This work specifically concentrates on developing testbeds for the impact of position errors on position-assisted distributed beamforming in WSNs. Various network topologies and techniques will be assessed to study the behaviour of the systems in different scenarios.

Keywords: Wireless System Networks, Multiple Input Multiple Output, Distributed Beamforming, Communications & Sensing, Signal Processing

“Se a vida te der limões, faz um sumo de pêra. Vai toda a gente ficar impressionada.”

— Panda, *Panda do KungFu 4*

Contents

Acknowledgements	ii
Resumo	iv
Abstract	v
List of Acronyms	xi
List of Figures	xiii
1 Introduction	1
1.1 Motivation	1
1.2 Objectives and Contributions	2
1.3 Assumptions of the model	3
1.4 Dissertation Outline	3
2 Concepts	5
2.1 Wireless Sensor Networks	5
2.2 Near-Field and Far-Field	7
3 Beamforming	10
3.1 Conventional Beamforming	10
3.1.1 Two-element array	11
3.1.2 Uniform Linear Array	14
3.1.3 Linear Phased Array	17
3.1.4 Planar Array	18
4 Distributed and Collaborative Beamforming	22

4.1	Distributed Linear Array	22
4.2	Distributed Planar Array	24
4.3	Position-based distributed beamforming: system model and simulation testbed	26
4.4	Near-Field Distributed Beamforming Ideal Scenario	27
4.5	Impact of Sensor Position Error in Near-Field Distributed Beamforming . . .	32
4.5.1	Sensor Position Error and Signal Degradation	33
4.6	Impact of Base Station Position Error in Near-Field Distributed Beamforming	35
4.7	Receiver Position Impact in Signal Quality in Near-Field Scenarios	38
4.8	Impact of Received Power Adjustment in Near-Field Distributed Beamforming	44
4.9	Far-Field Distributed Beamforming Ideal Scenario	49
4.10	Multiple groups scenario	52
5	Conclusions	57
5.1	Future Work	58
6	Bibliography	59

List of Acronyms

AoA	Angle of Arrival
AoD	Angle of Departure
AF	Array Factor
BP	Beampattern
BS	Base Station
CPU	Central Processing Unit
DCBF	Distributed and Collaborative Beamforming
DoA	Direction of Arrival
EP	Element Pattern
HPBW	Half Power Beam Width
IoE	Internet of Everything
IoT	Internet of Things
ToA	Time of Arrival
LIS	Large Intelligent Surface
LOS	Line-Of-Sight
MIMO	Multiple-Input Multiple-Output
RSSI	Received Signal Strength Indicator
SNR	Signal-Noise Ratio

ULA	Uniform Linear Array
URA	Uniform Rectangular Array
WSN	Wireless Sensor Network

List of Figures

2.1	Sensor nodes scattered in a sensor field [1].	6
2.2	Spherical wavefront approaches a flat receive antenna array [4].	7
2.3	Square Antenna Array $L \times L$	8
2.4	Antenna near and far field regions [22].	9
3.1	Beamforming technique from [25].	10
3.2	Two-elements array [30].	12
3.3	Two-element array radiation pattern with $d = \frac{\lambda}{4}$ spacing align along horizontal axis.	14
3.4	Uniform Linear Array example	15
3.5	N -element array beampattern for a different number of elements normalized by the number of sensors with $d = \frac{\lambda}{2}$	16
3.6	N -element array beampattern for difference spacing between elements normalized by the number of sensors.	17
3.7	N -element array beampattern for different θ_{max} values normalized by the number of sensors.	18
3.8	Typical configuration of planar antenna array with four-elements [16].	19
3.9	5x5 Planar Array.	20
3.10	5x5 Planar Array 3D Radiation Pattern.	20
3.11	Radiation Pattern components.	21
4.1	Distributed Linear Array examples and respective beampatterns.	24
4.2	Distributed Planar Array example.	25
4.3	Radiation Pattern components of a Distributed Planar Array.	26
4.4	Schematic of Testbed.	27

4.5	Distributed WSN with 20 nodes randomly placed.	28
4.6	Time of arrival of each signal, for scenario in Fig. 4.5 at frequency $f_c = 3\text{GHz}$	29
4.7	Phase-compensated signals at the receiver.	29
4.8	Received ideal signal for a WSN with 20 nodes randomly placed nodes.	30
4.9	Signal attenuation of each sensor for the scenario of Fig. 4.5, when the Base Station (BS) (drone) is at a height of 20λ	31
4.10	Received attenuated signal for a WSN with 20 nodes randomly placed nodes.	32
4.11	Schematic of Testbed Sensors Position Error.	32
4.12	Distributed WSN with 20 nodes randomly placed with node position error.	33
4.13	Distributed WSN with 20 nodes randomly placed with position error.	33
4.14	Normalized amplitude boxplot of distributed WSN with 20 nodes randomly placed with position error.	34
4.15	Schematic of Testbed Drone Position Error.	35
4.16	Distributed WSN with 20 nodes randomly placed with drone position error.	36
4.17	Normalized amplitude boxplot of distributed WSN with 20 nodes randomly placed with position error in the receiver 0.025λ to 2.975λ	37
4.18	Normalized amplitude boxplot of distributed WSN with 20 nodes randomly placed with position error in the receiver 3.025λ to 3.975λ	37
4.19	All drone possible positions in a 25×25 field.	39
4.20	The 4 scenario used to test drone optimum position.	39
4.21	Colormaps for the 4 scenario studied.	40
4.22	Normalized amplitude boxplot of distributed WSN with 20 nodes randomly placed with position error in the receiver 0.025λ to 2.975λ	43
4.23	Normalized amplitude boxplot of distributed WSN with 20 nodes randomly placed with position error in the receiver 3.025λ to 3.975λ	44
4.24	Transmission amplitude by each sensor.	45
4.25	Received signals with amplitude adjusted.	46
4.26	Total received signal with amplitude adjusted.	46
4.27	Normalized amplitude boxplot of distributed WSN with 20 nodes randomly placed with the sensors' position error.	47

4.28 Normalized amplitude boxplot of distributed WSN with 20 nodes randomly placed with the drone's position error with adjusted amplitude.	48
4.29 Distributed WSN with 20 nodes randomly placed.	49
4.30 Field beampattern.	50
4.31 Signal attenuation of each sensor.	50
4.32 Time of arrival of each signal.	51
4.33 Phase-compensated signals at the receiver.	51
4.34 Total received signal.	52
4.35 Distributed WSN with 5 clusters of sensors randomly placed with drone position error.	52
4.36 Phase-compensated signals at the receiver.	53
4.37 Total received signal with phase-compensated approximated to the sensors' exact position.	53
4.38 Phase-compensated approximated to the center of mass signals at the receiver.	54
4.39 Total received signal with phase-compensated approximated to the center of mass.	55
4.40 Effect of drone moving from the sensor in the far-field approximation.	55

1 Introduction

A Wireless Sensor Network (WSN) is an interconnected collection of sensor nodes designed to detect one or more aspects of the physical environment, such as temperature, sound, chemical agents, and so on [7, 18]. Due to this, a WSN can be considered a distributed multi-user Multiple Input Multiple Output (MIMO) system when connecting to a multiple-antenna Base Station(BS) serving as a gateway.

1.1 Motivation

Multiple-Input Multiple-Output (MIMO) systems leverage multiple antennas to combat path loss, a signal-weakening phenomenon especially prevalent in free space at higher frequencies [20]. This capability becomes particularly attractive for WSN as distributed MIMO. In our work, we explore utilizing WSNs comprised of numerous low-power sensors randomly distributed across a field, effectively creating a distributed MIMO system.

WSNs might have high development costs upfront, but their implementation costs are remarkably low. This advantage helps balance the initial investment, making WSNs a financially viable solution for various applications. The low implementation cost allows for deployment in scenarios where traditional infrastructure is impractical or expensive. For instance, WSNs can be used for environmental monitoring, replacing the need for costly fixed-point stations [21].

However, the limited range of low-energy sensors would benefit from beamforming for effective information transmission. This is because each group of sensors, strategically positioned across the area, will collaborate to create a beamforming pattern. This pattern effectively concentrates transmission energy in a specific direction, enhancing signal strength and range, thereby enabling efficient information transmission despite the sensors' limited individual range.

Optimizing transmission in our WSN necessitates thoroughly understanding beamform-

ing principles. This knowledge encompasses the techniques for creating constructive beams, which are crucial for focusing the signal in WSNs, and the impact of transmitter distance on phase compensation.

As previously noted, the sensors in the network are deployed randomly. This inherent randomness poses a significant challenge in obtaining accurate localization information for distributed networks. The precision of sensor localization is paramount for achieving constructive beamforming.

1.2 Objectives and Contributions

Beamforming is a well-studied technique particularly advantageous for Uniform Rectangular Array (URA), like Large Intelligent Surface (LIS), due to their inherent geometric properties, of symmetry and regularity in antenna spacing.

However, it is still a challenge for randomly distributed WSNs. This is because, in this network type, we don't know the exact node's position, making it more difficult to apply beamforming, or Distributed and Collaborative Beamforming (DCBF) techniques more specifically, in these cases. These networks also suffer from the problem that they are designed to be applied in environments that may change, which requires an in-depth study of the localization methods used, as studied in [27].

Our first objective is to understand how Conventional Beamforming is implemented by leveraging the knowledge from existing research on unidirectional arrays like Uniform Linear Array (ULA) and in bi-directional arrays such as URA.

Thus, using the previous concept, by constructing arrays with varying element spacing, we will explore how sensor phase adjustments can be utilized to achieve optimal beamforming performance for DCBF techniques.

Following the investigation of constructive beamforming techniques, we will study the effect of position estimation errors in our systems. These errors are expected to reduce the power of our received signal since our transmitter will not have the correct phase to achieve the most efficient constructive beamforming.

To achieve this objective, we analyze various array configurations using MATLAB software [11–13]. This approach ensures data reliability, and all graphical representations are generated from custom code developed within the software.

1.3 Assumptions of the model

Certain assumptions and limitations were established at the outset of this work to facilitate the tractability of the analysis. Firstly, the sensor nodes were modelled as employing isotropic antennas. Isotropic antennas radiate uniformly across all spatial directions, resulting in equal signal strength throughout their spherical radiation pattern. Secondly, it was assumed that all sensors were synchronized and operated on a common transmission frequency. Finally, the transmitters and receiver are always in Line-Of-Sight (LOS) and signal degradation, such as shadowing and reflection, will not be considered.

1.4 Dissertation Outline

Having established the background and motivation for this research, let's delve into the structure of this dissertation.

Chapter 2 introduces the concepts of WSNs and near-field and far-field, which are crucial concepts for this work.

Chapter 3 provides a comprehensive overview of beamforming techniques. Section 3.1, titled "Conventional Beamforming," offers a foundational discussion. Section 3.1.1, "Two-Element Array," demonstrates basic beamforming concepts using a simple two-element configuration. Building upon this foundation, Section 3.1.2, "N-Element Array," explores beamforming with arrays containing N elements. Section 3.1.3, "Phased Array," delves into phased arrays, discussing methods for steering the main beam of the system. Finally, Section 3.1.4, "Planar Arrays," introduces planar arrays, which expand sensor placement onto a new axis.

Building upon the foundational concepts established in previous sections, Chapter 4, titled "Distributed and Collaborative Beamforming," explores this technique. It delves into applications for both unidirectional arrays (Section 4.1) and bidirectional arrays (Section 4.2), investigating the effects of varying node spacing within these configurations. Section 4.4 investigates a baseline scenario with the known receiver and transmitter positions to understand the received signal's behaviour. Leveraging on this, subsequent sections introduce controlled errors. Section 4.5 examines the impact of sensor errors, while Section 4.6 analyzes the effects of drone position errors. These sections explore how these errors affect signal degradation. Section 4.7 employs an exhaustive search algorithm to find the optimal

drone position, verifying the results obtained in the previous section on drone position errors. Section 4.8 presents the impact of amplitude adjustments of the transmitted signal to arrive the receiver with the same amplitude. Section 4.9 presents the benefits of operating in the far-field region, analyzing signal behaviour with and without phase compensation. Finally, Section 4.10 presents a scenario with several clusters of sensors being the main objective of studying near-field and far-field behaviour in this type of scenario.

In the end, Chapter 5 concludes this dissertation and proposes possible future work which can be done in this area.

2 Concepts

This chapter lays the groundwork for the remainder of this dissertation by introducing the fundamental concepts that will be utilized throughout the analysis. We begin by exploring the core concept of WSNs. As the primary system of focus in this work, we will provide a comprehensive definition and outline the key characteristics of WSNs and their applications. Subsequently, the chapter delves into the near-field and far-field regions, establishing clear definitions and the differences in operating in each region.

2.1 Wireless Sensor Networks

Wireless Sensor Networks (WSNs) are networks comprising numerous low-cost miniature sensors communicating wirelessly. These tiny sensor nodes, called motes, typically integrate sensing, data processing, and communication capabilities. The core strength of WSNs lies in their collaborative nature, leveraging the combined power of many nodes to achieve a comprehensive sensing task. This collaborative approach offers significant advantages over traditional sensor deployments, which can be categorized into two main approaches as documented in [1, 14].

- **Centralized Sensor Deployment:** In this traditional method, sensors can be positioned far from the actual phenomenon of interest. These sensors are typically large and require complex techniques to distinguish the target signal from environmental noise. Due to their complexity, these sensors can be expensive and require significant maintenance.
- **Distributed Sensor Deployment:** The other traditional approach involves deploying several smaller, simpler sensors that focus solely on sensing the phenomenon. The positions of these sensors and the communication topology between them are carefully planned and engineered. These sensors typically transmit raw data, often in the form of

time series, to central nodes for processing and data fusion. While this approach can be more cost-effective, it requires a robust communication infrastructure and centralized processing capabilities.

Fig. 2.1 shows a WSN where every sensor communicates individually to a receiver.

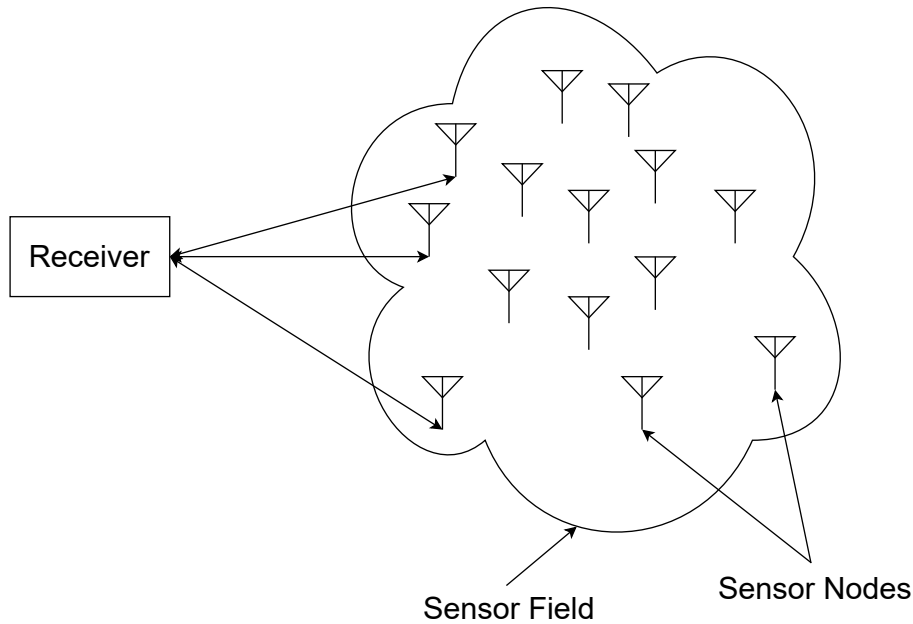


Figure 2.1: Sensor nodes scattered in a sensor field [1].

Due to their practicality and low cost, WSNs have emerged as a powerful tool for various applications [8]. Their ability to gather and transmit data wirelessly makes them well-suited for scenarios where traditional wired infrastructure might be impractical or expensive, such as:

- **Military target tracking and surveillance:** They excel at detecting and reporting spatially correlated movements, such as those associated with coordinated troop and tank deployments, in military target tracking and surveillance, specifically aiding in intrusion detection and identification [8, 32].
- **Environmental monitoring:** They can be deployed for tasks such as seismic sensing, as referenced in [8, 29], or natural disaster relief, as shown in [6, 8]. With natural disasters they can detect and analyse environmental changes, enabling the prediction of disasters before they strike or being an important help in rescue missions.

- **Healthcare applications:** Their potential in healthcare applications is promising. On biomedical health monitoring, surgical implants of sensors can help monitor a patient's health as highlighted in [8, 9].
- **Smart cities:** They have a vital role in shaping the Internet of Things (IoT) or Internet of Everything (IoE). WSNs can be implemented in several areas such as room temperature and humidity, monitoring street activity, buildings stability and reliability, and water quality and pipeline spillage monitoring in Water Distribution Networks [17].

Despite their diverse applications, WSNs face several limitations that necessitate ongoing development. Key areas for improvement include new algorithms, improved communication protocols, low-power modules, robust cybersecurity measures, and more. Additionally, challenges remain in localization and synchronization methods, which can hinder the usability of these systems.

2.2 Near-Field and Far-Field

During this work, the concepts of near-field and far-field regions surrounding an electromagnetic wave source will be presented. These regions define the zones where the behavior of the electromagnetic field exhibits distinct characteristics. We will explore the key differences in working within these two fields, highlighting the implications for antenna characterization, and signal propagation. Fig. 2.2 shows an example of a spherical wavefront approaching a flat antenna array with dimensions L , comprised of individual antennas with dimensions x . This schematic will serve as the foundation for the near-field and far-field examples discussed in this section.

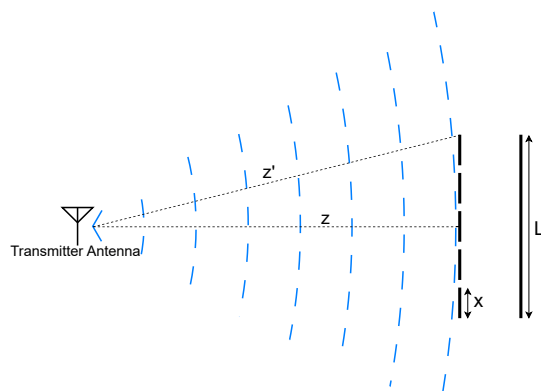


Figure 2.2: Spherical wavefront approaches a flat receive antenna array [4].

The far-field region of an antenna array represents the area where the electromagnetic waves propagate essentially as plane waves. The wavefronts in the far-field are considered parallel, simplifying calculations and analysis [4]. This characteristic allows us to approximate an antenna array, under certain conditions, as a single point source when calculating its radiation pattern in the far-field [2].

To ensure dominance of plane waves and achieve this far-field behavior, a minimum distance from the antenna (or array) must be maintained. This minimum distance is known as the Fraunhofer distance and can be calculated using [4].

$$d_f \geq \frac{2L^2}{\lambda}. \quad (2.1)$$

where L is the dimension of our antenna array side and λ the wavelength, as shown in Fig. 2.3.

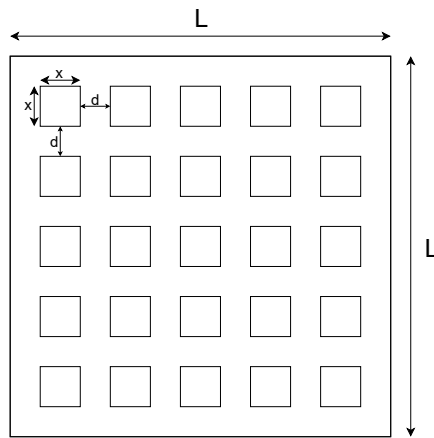


Figure 2.3: Square Antenna Array $L \times L$.

Using this concept, the minimum distance d_f in Fig. 2.2 at 3GHz frequency and for $L=10\lambda$ is 20 meters.

Conversely, near-field is achieved when the distance between the transmitter and the receiver is less than the Fraunhofer distance and has as primary characteristics the following phenomena [4]:

- Different distances to antennas
- Different effective areas
- Different polarization losses

Besides that, near-field can be separated into two parts. The radiative near-field is an intermediate region where the propagation distance to the receiver is too short to neglect the phase and/or amplitude variations over the receive antenna, but large enough to ignore direct hardware interaction between the transmitter and receiver. The reactive near-field is closest to the transmitter and includes additional electromagnetic effects such as evanescent waves and magnetic induction [4]. Fig. 2.4 illustrates these antenna field regions division.

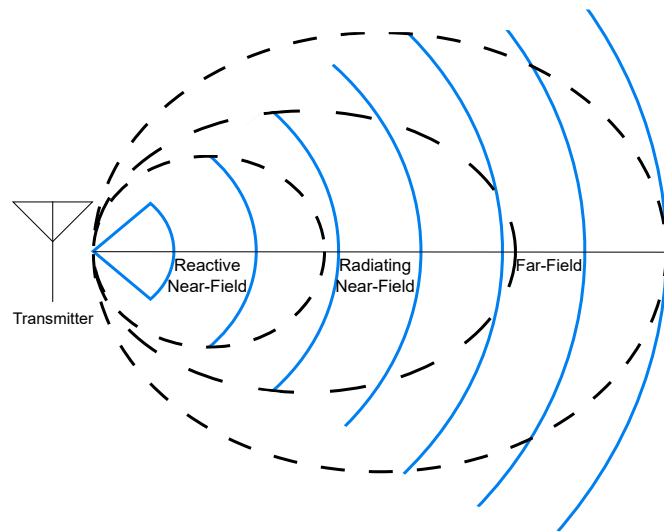


Figure 2.4: Antenna near and far field regions [22].

3 Beamforming

This chapter introduces the concept of beamforming, a crucial technique in MIMO wireless communication systems, by providing a concise explanation and examples of Conventional Beamforming. It is an essential concept for understanding the behaviour of linear and planar models.

Beamforming is achieved by manipulating the phase of the transmitted or receiver signal. By adjusting the phase of the signal of different antennas, the beam can be coherently combined allowing to focus energy in a given specific direction, as shown in Fig. 3.1.

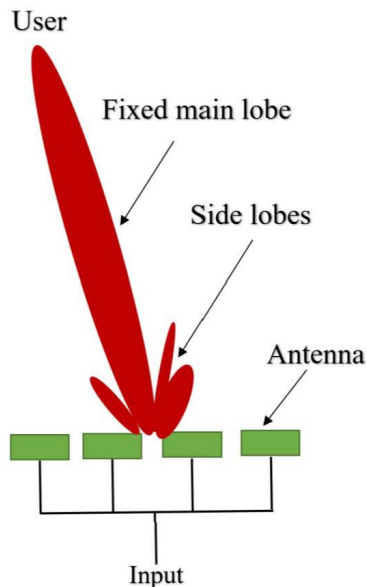


Figure 3.1: Beamforming technique from [25].

3.1 Conventional Beamforming

Beamforming is a versatile and powerful approach to receiving, transmitting, or relaying signals in a spatially selective way in the presence of interference and noise [10]. It can be

used for plenty of different purposes, such as detecting the presence of a signal, estimating the Direction of Arrival (DoA) and enhancing the signal's Signal-Noise Ratio (SNR) [3].

To create a proper beamforming, we must synchronize the transmitters. The synchronization process is to delay/advance each transmitter output by a time so that the signal components coming from a desired direction are synchronized, creating constructive beamforming that enhances the signal [3].

The difference between Conventional Beamforming and Distributed and Cooperative Beamforming is the uniform space between antennas, that is assumed for the first case, while in the second case it is variable. Thus, in this section, we address the first one by considering three types of antenna arrays: two-element arrays, N -element arrays, and phased arrays. Analyzing these conventional configurations will provide a foundation for understanding the principles of distributed beamforming.

Antenna arrays exhibit a far-field radiation pattern demonstrably distinct from a single antenna. This pattern, quantified by the complex-valued Array Factor (AF), arises from the combined radiation characteristics of N individual radiators within the array. To facilitate mathematical analysis, several simplifying assumptions are commonly employed [2]:

- all radiators are identical in every respect;
- the radiators are uniformly spaced throughout the array;
- there is a constant signal phase shift between adjacent radiators.

The equation that describes the array factor of an antenna array depends on several factors, including the number of antenna elements (N), element spacing (d) between these, amplitude excitation coefficients (I_n), observation direction (θ, ϕ), the difference in phase excitation between the elements (β) and the wave vector (k). With this, the general equation for the array factor of a linear antenna array is given [2]

$$AF = \sum_{n=0}^{N-1} I_n e^{(jkn \cdot d \cos(\theta) + \beta)}. \quad (3.1)$$

3.1.1 Two-element array

Two-element arrays offer the most straightforward configuration for beamforming. However, it's crucial to differentiate near-field regions from far-field regions. Each element in the

array will have a distinct distance to the reference point in the near-field since the distance between them can't be overlooked, resulting in various Angle of Departure (AoD), as shown in Fig. 3.2a. Conversely, in the far-field, the array can be effectively reduced to a single point with a constant distance, d , from a unique AoD, θ , as illustrated in Fig. 3.2b.

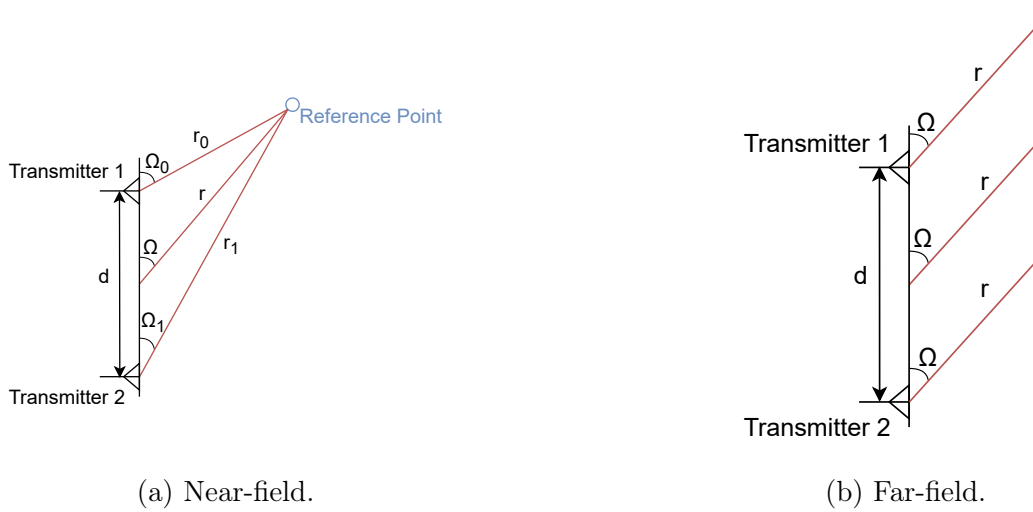


Figure 3.2: Two-elements array [30].

Assuming in Fig. 3.2 that the antenna under investigation is an array of two infinitesimal horizontal dipoles positioned along the z -axis, as shown in [2], the total field of the array is equal to the field of a single element positioned at the origin multiplied by a factor, which is widely referred to as the AF. The total field radiated by the two-element array, The total field is the sum of both elements' fields in the y - z plane, assuming no interaction between them, given by [2]

$$\mathbf{E}_t = \mathbf{E}_1 + \mathbf{E}_2 = \hat{\mathbf{a}}_\theta j\eta \frac{kI_0\ell}{4\pi} \left\{ \frac{e^{-j[kr_1 - (\beta/2)]}}{r_1} \cos \theta_1 + \frac{e^{-j[kr_2 - (\beta/2)]}}{r_2} \cos \theta_2 \right\}. \quad (3.2)$$

where \mathbf{E}_t is the total field radiated by the two elements, \mathbf{E}_1 and \mathbf{E}_2 represent the field radiated by each dipole element, $\hat{\mathbf{a}}_\theta$ is the radial unit vector, η is the intrinsic impedance of the medium, k denotes the wave vector, I_0 is a constant that describes the wave current amplitude, ℓ is the length of the dipole, r_1 and r_2 denote the distance between dipole 1 and dipole 2 to the reference point, and β denotes the difference in phase excitation between the elements.

Assuming far-field conditions observed in Fig. 3.2b [2]:

$$\theta_1 \simeq \theta_2 \simeq \theta \quad (3.3a)$$

$$\left. \begin{array}{l} r_1 \simeq r - \frac{d}{2} \cos \theta \\ r_2 \simeq r + \frac{d}{2} \cos \theta \end{array} \right\} \text{for phase variations} \quad (3.3b)$$

$$r_1 \simeq r_2 \simeq r \rightarrow \text{for amplitude variations} \quad (3.3c)$$

By substituting in (3.2), we can obtain [2]:

$$\mathbf{E}_t = \hat{\mathbf{a}}_\theta j \eta \frac{k I_0 l e^{-jkr}}{4\pi r} \cos \theta \times \left\{ 2 \cos \left[\frac{1}{2} (kd \cos \theta + \beta) \right] \right\}. \quad (3.4)$$

In (3.4), the left part of the product is the radiation field of a single dipole. The right part describes the radiation pattern of the array, called array factor [30]. Thus, in constant amplitude two-element arrays, it is possible to obtain the AF using (3.5):

$$AF = 2 \cos \left[\frac{1}{2} (kd \cos \theta) + \beta \right] \quad (3.5)$$

where $k = 2\pi/\lambda$ is the wave vector that characterizes the direction of the wave propagation, d is the distance between the elements, and β signifies the introduced phase difference between the signals at each element. This phase difference allows for control of the beam direction in beamforming and will be more studied in Section 3.1.3.

More generally, for a regular antenna aggregate, the array radiation pattern, also denoted as Beampattern (BP), is defined as the product of the radiation pattern of each antenna element, i.e. Element Pattern (EP), by the antenna aggregate AF, this is:

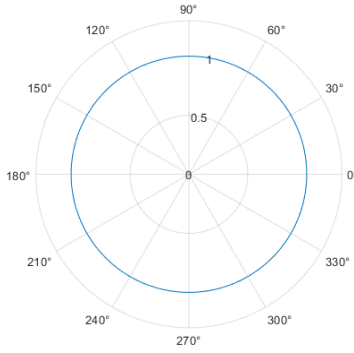
$$BP = EP \times AF. \quad (3.6)$$

To better illustrate (3.6), the normalized pattern of an isotropic element, the AF, and the BP for the two-element array of Fig. 3.2b (i.e. in the Far-field) are shown in Fig. 3.3.

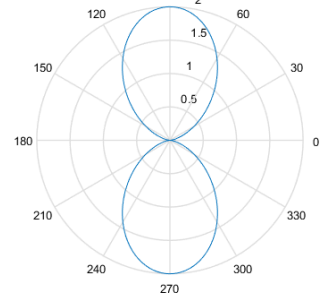
Since the transmitters used in this work were idealised as isotropic, i.e. $EP = 1$ as seen in Fig. 3.3a, it results that

$$BP = AF. \quad (3.7)$$

Fig. 3.3 also shows, that with the antenna-elements aligned along the horizontal axis, this array has no radiation along this axis, and the maximum radiation is along the vertical axis, i.e. orthogonal one.

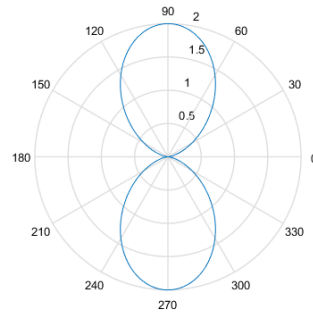


(a) Element pattern.



(b) Array Factor.

\equiv



(c) BeamPattern.

Figure 3.3: Two-element array radiation pattern with $d = \frac{\lambda}{4}$ spacing align along horizontal axis.

3.1.2 Uniform Linear Array

Uniform Linear Array (ULA) refers to an array of N -element, usually $N > 2$, linearly aligned along a single direction, and with equal spacing between antenna elements, typically $\frac{\lambda}{4}$ or $\frac{\lambda}{2}$. Fig. 3.4 shows an example of a ULA, being all the systems linear with the same orientation.

Assuming all elements in the array have identical signal amplitude and behave as isotropic point sources, the AF can be given by [30]:

$$AF = (1 + e^{j\psi} + \dots + e^{j(N-1)\psi}) = \sum_{n=0}^{N-1} e^{j n \psi}. \quad (3.8)$$

where ψ is defined by:

$$\psi = kd \cos \theta. \quad (3.9)$$

Another way to express this array factor, if the reference element is in the center of the array [30]:

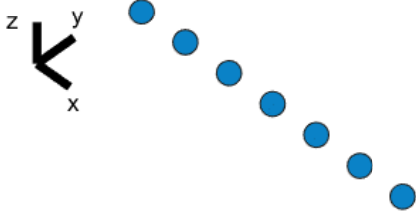


Figure 3.4: Uniform Linear Array example

$$AF = \frac{\sin\left(\frac{N}{2}\psi\right)}{\sin\left(\frac{1}{2}\psi\right)}. \quad (3.10)$$

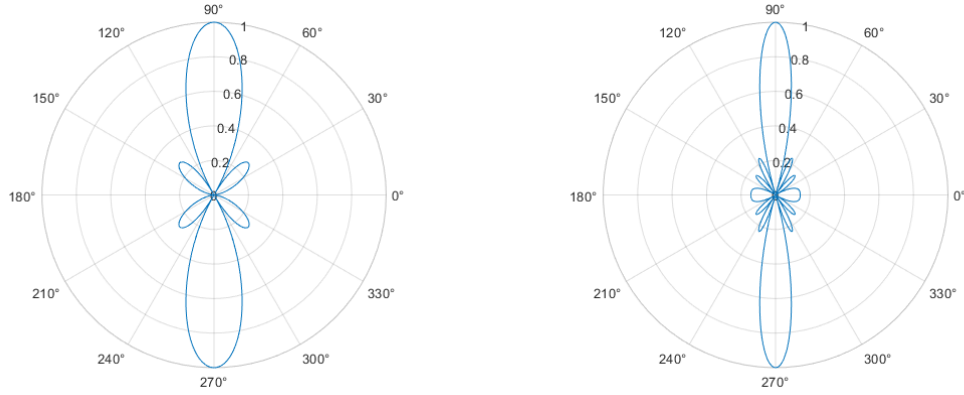
The normalized AF, denoted as AF_N , is obtained by dividing (3.10) by N , because the maximum value for the AF is given by the number of antenna elements, i.e. N , and so

$$AF_N = \frac{1}{N} \frac{\sin\left(\frac{N}{2}\psi\right)}{\sin\left(\frac{1}{2}\psi\right)}. \quad (3.11)$$

As mentioned before, if the number of sensors and the distance between them vary, it originates different BPs in the system. In Fig. 3.5 the BP for arrays with different numbers of elements is shown when setting $d = \frac{\lambda}{2}$, while in Fig. 3.6 it is shown when varying the distance between sensors for a fixed 7-element array.

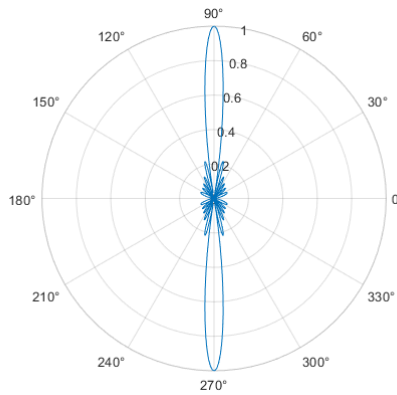
In Fig. 3.5, we can observe that the main beam narrows and has more power as the number of sensors increases, as expected. However, there are also smaller lobes in other directions, known as side lobes. These side lobes represent energy unintentionally radiated outside the desired main beam direction [28], which can cause, for example, privacy problems.

In Fig. 3.6, the element spacing within a linear antenna array significantly influences its radiation pattern. The concept of the far-field approximation can explain this phenomenon. In the far field, the wavefronts from each element in the array are essentially considered parallel. The closer spacing between elements can also be viewed as approximating a single, larger antenna aperture. As the aperture size increases, the main beam width widens according to the principles of diffraction. Additionally, a more closely spaced array can decrease the number of side lobes present in the array factor. This is because the closer spacing allows for a more gradual transition in the radiation pattern, reducing the occurrence of sharp peaks and nulls contributing to side lobes.



(a) $N = 4, AF_{max} = 4.$

(b) $N = 7, AF_{max} = 7.$



(c) $N = 12, AF_{max} = 12.$

Figure 3.5: N -element array beampattern for a different number of elements normalized by the number of sensors with $d = \frac{\lambda}{2}$.

In the arrays shown in this section, the main direction of the signal propagates perpendicularly to the array axis, where the majority of the transmitted energy is concentrated, forming the main lobe.

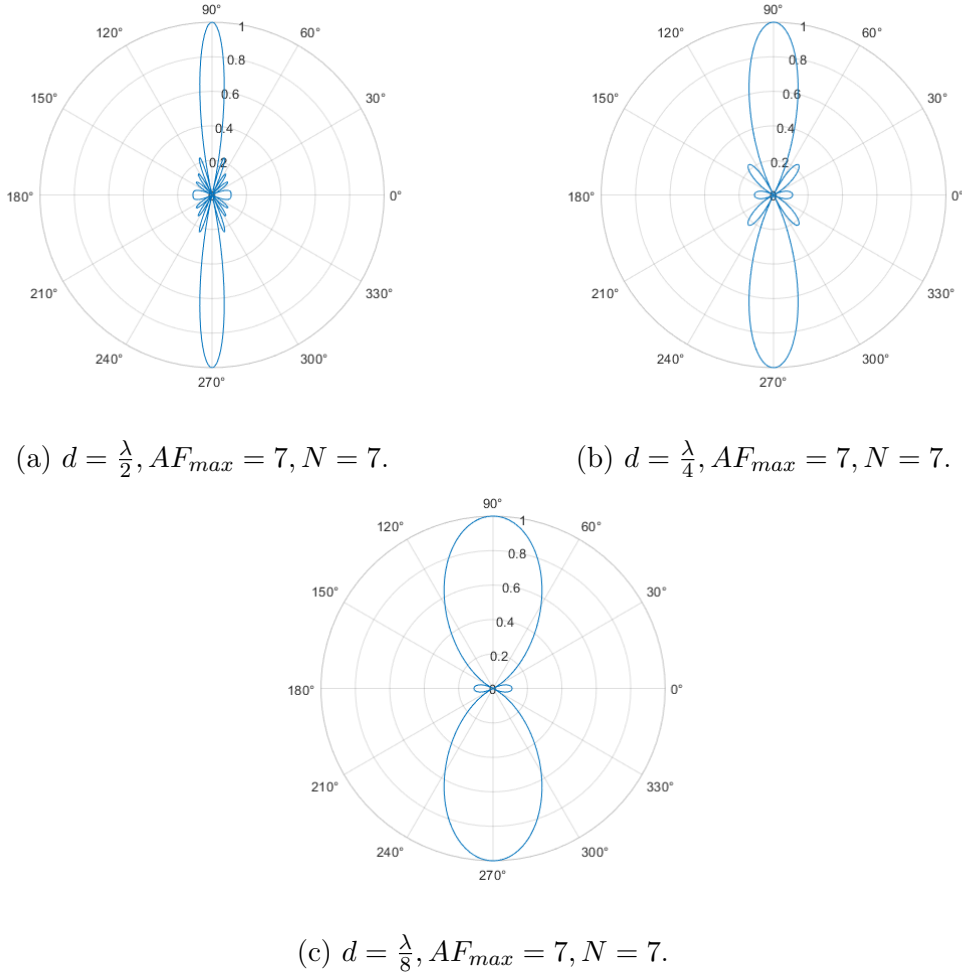


Figure 3.6: N-element array beampattern for difference spacing between elements normalized by the number of sensors.

3.1.3 Linear Phased Array

Generally, a phased array is an array of antennas in which we can change the signal's direction electronically by manipulating the signal's phase at each antenna element without physically moving the transmitters themselves.

Being k and d system parameters, and θ_{max} the main beam direction, the value of β can be determined by:

$$\beta = -kd \cos \theta_{max}. \quad (3.12)$$

This value will be applied at (3.9), being ψ now obtained by:

$$\psi = kd \cos \theta + \beta \quad (3.13)$$

Applying (3.13) to (3.11), it is possible to obtain the AF of the phased array. If the objective is to obtain a beam pointing to $\pi/4$ using an array with parameters $N = 7$,

$d = \lambda/2$, we will get our $\beta = \pi/\sqrt{2}$. Thus, using 3.1 for different β values, we obtained the graphs shown 3.7.

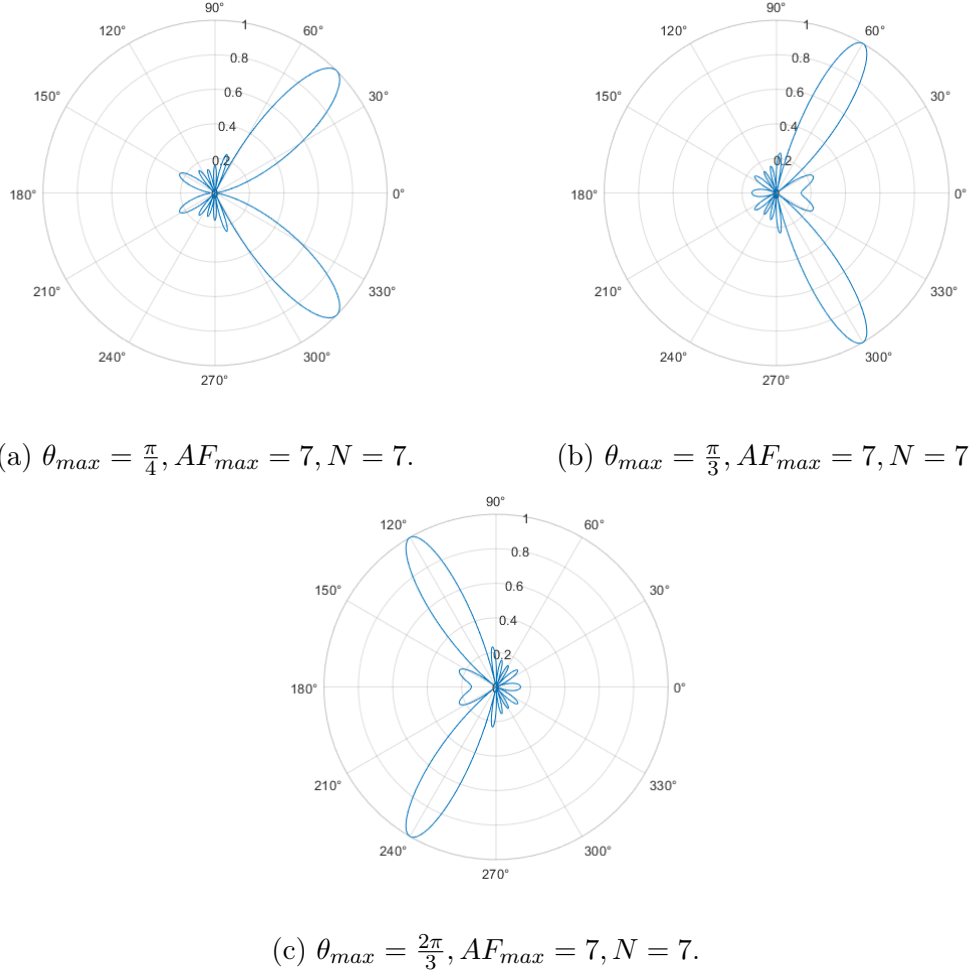


Figure 3.7: N-element array beampattern for different θ_{max} values normalized by the number of sensors.

As is possible to analyse, the number of side lobes remains similar for the different θ_{max} values, and the maximum side lobe is similar in every case also.

3.1.4 Planar Array

As the name suggests, a planar array, Uniform Rectangular Array (URA), consists of M rows and N columns of antennas ($M \times N$) distributed coplanarly with uniform spacing between elements.

One example of a planar array, based in [16], is a symmetrical configuration with $L \times L$ elements, as illustrated in Fig. 3.8. The four elements are arranged in a square pattern within the 2×2 grid.

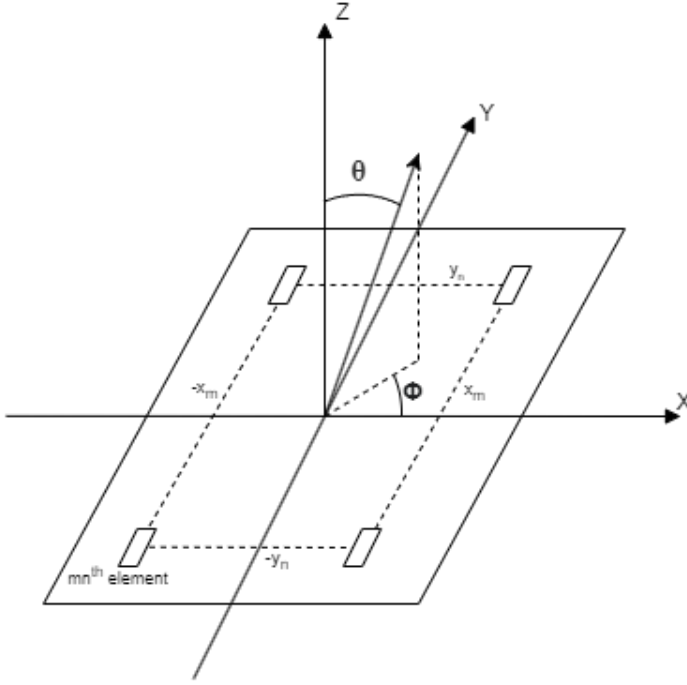


Figure 3.8: Typical configuration of planar antenna array with four-elements [16].

To calculate the radiation pattern of the planar array, we need to consider the distance between elements, d , and the coordinates (x_m, y_n) of each antenna element within the $L \times L$ grid. For the mn^{th} element the coordinates are given by (md, nd) , respectively. Conversely, for an even number of elements, L , these coordinates become $(m - 0.5)d$ and $(n - 0.5)d$, respectively. (3.14) and (3.15) provide the radiation pattern for odd and even L , respectively [16].

$$AF_{odd}(\Psi_x, \Psi_y) = \sum_{m=-T}^T \sum_{n=-T}^T I_{mn} e^{j(m\Psi_x + n\Psi_y)}, \quad T = \frac{L-1}{2} \quad (3.14)$$

$$AF_{even}(\Psi_x, \Psi_y) = \sum_{\substack{m=-T \\ m \neq 0}}^T \sum_{\substack{n=-T \\ n \neq 0}}^T I_{mn} e^{j((m \pm 0.5)\Psi_x + (n \pm 0.5)\Psi_y)}, \quad T = \frac{L}{2} \quad (3.15)$$

where I_{mn} is the excitation current of the mn^{th} element and Ψ_x and Ψ_y are real variables defined by [16, 23]:

$$\Psi_x = kd(\sin \theta \cos \phi - \sin \theta_{max} \cos \phi_{max}) \quad (3.16)$$

$$\Psi_y = kd(\sin \theta \sin \phi - \sin \theta_{max} \sin \phi_{max}) \quad (3.17)$$

being the main beam azimuth and elevation given by θ_{max} and ϕ_{max} , respectively.

Since generating a 3D radiation pattern through code can be challenging, the MATLAB App Sensor Array Analyzer [12] was employed to visualize the radiation patterns of 5x5 planar arrays, shown in Fig. 3.9.

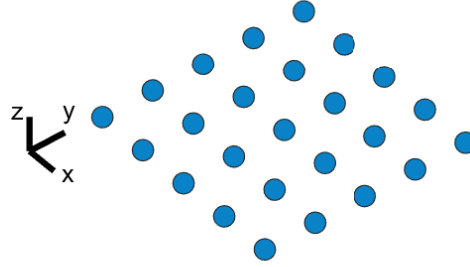


Figure 3.9: 5x5 Planar Array.

Within the app, the element spacing (d) was set to 0.5λ , the operating frequency (f) to 1 GHz, and the z-axis was designated as the normal to the planar array, obtaining Fig. 3.10.

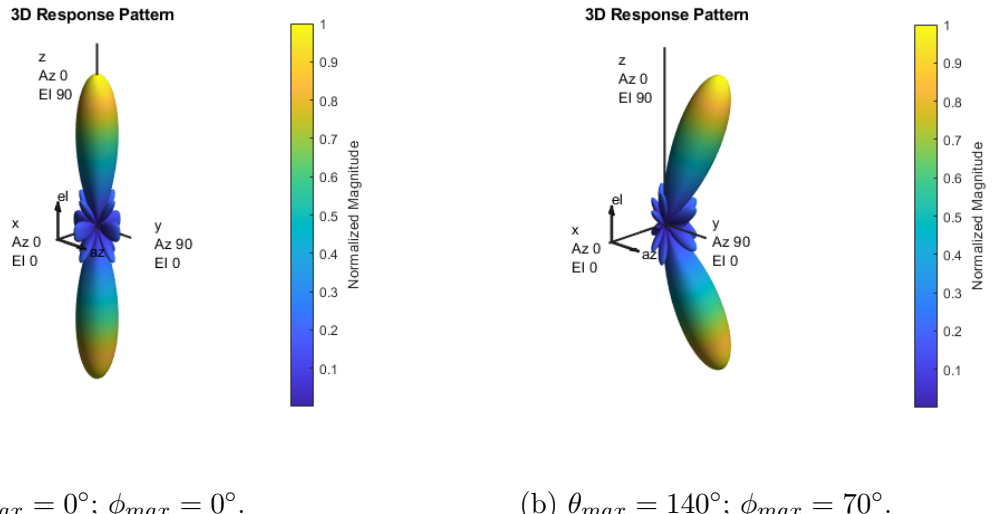
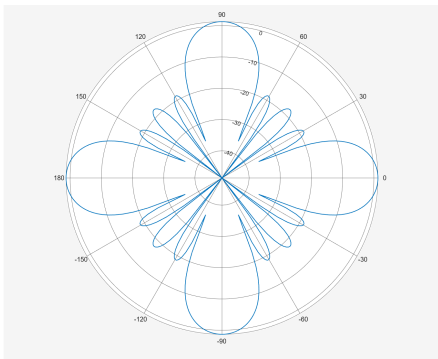
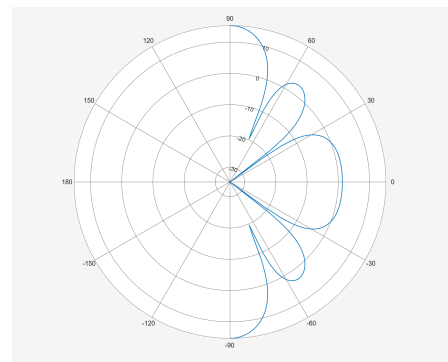


Figure 3.10: 5x5 Planar Array 3D Radiation Pattern.

This array type introduces a new dimension to the radiation pattern beyond the previously discussed azimuth. This additional component is called elevation. Figs. 3.11a and 3.11b illustrate these two distinct components, which can be visualized by cutting through the 3D radiation pattern.



(a) Azimuth.



(b) Elevation.

Figure 3.11: Radiation Pattern components.

4 Distributed and Collaborative Beam-forming

Distributed and Cooperative Beamforming (DCBF) is a branch of cooperative communication where randomly located independent nodes cooperate to form a virtual antenna array in WSNs [15]. A WSN is an interconnected collection of sensor nodes designed to detect one or more aspects of the physical environment, such as temperature, sound, chemical agents, and so on [7, 18]. These characteristics made DCBF a promising technique to enhance wireless communication.

In contrast to conventional beamforming, DCBF finds application in WSNs with randomly spaced sensors. Here, the variable distances between sensors introduce uncertainty in their positions. This uncertainty can lead to issues when coherently combining the signals, potentially causing destructive beamforming.

In this section, using conventional beamforming's bases, adaptations will be made to the main equations introduced in Chapter 3 for conventional beamforming arrays to obtain the BP for a WSN with random space between elements. This BP study will be further developed by some different scenarios with randomly placed transmitters and a receiver in a square field under the assumption of perfect or slightly inaccurate knowledge of the sensors' position. These scenarios will be analysed to understand how position errors may affect DCBF efficiency.

4.1 Distributed Linear Array

By analyzing the equations presented in Section 3.1.3, it can be concluded that the distance between transmitters emerges as a critical factor in shaping a focused beam within a WSN. This highlights the challenge of achieving beamforming in distributed networks with variable sensor positions. Consequently, novel approaches are needed to account for these distance

variations and optimize distributed beamforming in WSNs.

The chosen coordinate system, shown in Figs. 4.1a and 4.1c, establishes a common reference point for achieving distributed beamforming. This reference point is the origin for calculating each transmitter's¹ distance, d_n . Subsequently, each transmitter's phase difference, β_n , is adjusted based on the desired beam direction, θ_{max} . By making the necessary adjustments to (3.12) we get:

$$\beta_n = -kd_n \cos \theta_{max}. \quad (4.1)$$

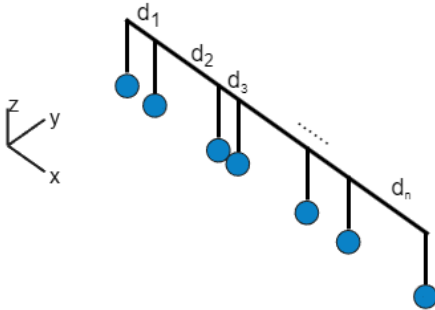
Thus, (3.8) served as the foundation for deriving (4.2), which was subsequently employed to compute the BP referent to linear arrays, with no uniform spacing between elements, shown in Figs. 4.1a and 4.1c, respectively.

$$AF = \sum_{n=0}^{N-1} e^{j(kd_n \cos \theta + \beta_n)} = \sum_{n=0}^{N-1} e^{j\psi_n}. \quad (4.2)$$

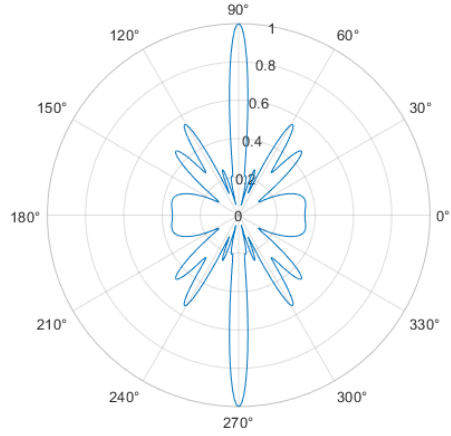
Assuming perpendicular radiation from the distributed linear array, the corresponding simulated normalized BP is presented in Figs. 4.1b and 4.1d.

In these two systems, while the main lobe exhibits desirable characteristics, such as good directivity and narrower beamwidth, the side lobes experience variable shape and typically an increase in Half Power Beam Width (HPBW) dependent on the non-uniform spacing pattern. This can be problematic in security-critical applications, where signal leakage towards unintended receivers should be minimized. It is essential to notice that, even though both systems, in Fig 4.1, have the same number of sensors, the varying distances between antenna elements lead to significant differences in the number and amplitudes of the side lobes, as evidenced by the BP.

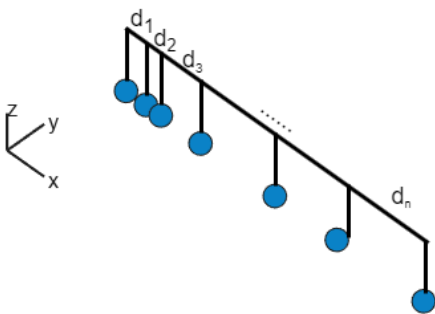
¹Henceforth, the term "transmitter" will be used interchangeably with "sensor" throughout this document.



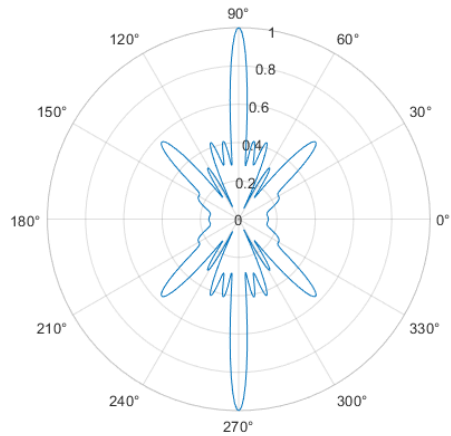
(a) System 1.



(b) System 1 Beampattern.



(c) System 2.



(d) System 2 Beampattern.

Figure 4.1: Distributed Linear Array examples and respective beampatterns.

4.2 Distributed Planar Array

Distributed planar arrays, where sensor elements are positioned randomly within a plane, present a unique challenge. Similar to conventional planar arrays, their complex element distribution makes calculating the array pattern computationally expensive. To address this, we employed a method similar to the one presented in Section 3.1.4 to analyse the radiation pattern of a distributed planar array example, as shown in Fig. 4.2, where, without loss of generalization, we assume that all sensors are within the xy plane.

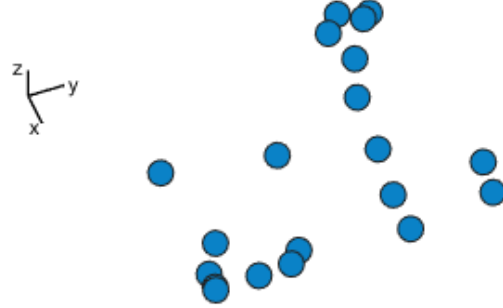


Figure 4.2: Distributed Planar Array example.

The presented example showcases a distributed planar array of 20 randomly positioned nodes. As in the distributed linear array some changes need to be made in the planar array conventional beamforming equations. Considering that d_m and d_n represent the distance between the transmitter located in (x_m, y_n) and the reference point in x and y-axis, respectively:

$$\Psi_{mx} = kd_m(\sin \theta \cos \phi - \sin \theta_{max} \cos \phi_{max}) \quad (4.3)$$

$$\Psi_{ny} = kd_n(\sin \theta \sin \phi - \sin \theta_{max} \sin \phi_{max}) \quad (4.4)$$

being possible calculate to calculate the AF using:

$$AF(\Psi_x, \Psi_y) = \sum_{m=-0}^{N-1} \sum_{n=-0}^{N-1} I_{mne} e^{j(\Psi_x + \Psi_y)} \quad (4.5)$$

As previously discussed, calculating the array pattern for such configurations is computationally demanding due to the random element distribution. This complexity can also lead to the formation of undesirable side lobes in the radiation pattern. Fig. 4.3a shows the radiation pattern for this specific system when the azimuth and elevation are equal to 0 degrees. This configuration causes our main lobe to be directed toward the normal of the sensors. Fig. 4.3b depicts the same planar array configuration where the primary beam is not directed towards the center, but instead the azimuth angle is intentionally set to 120 degrees, and the elevation angle is set to 45 degrees.

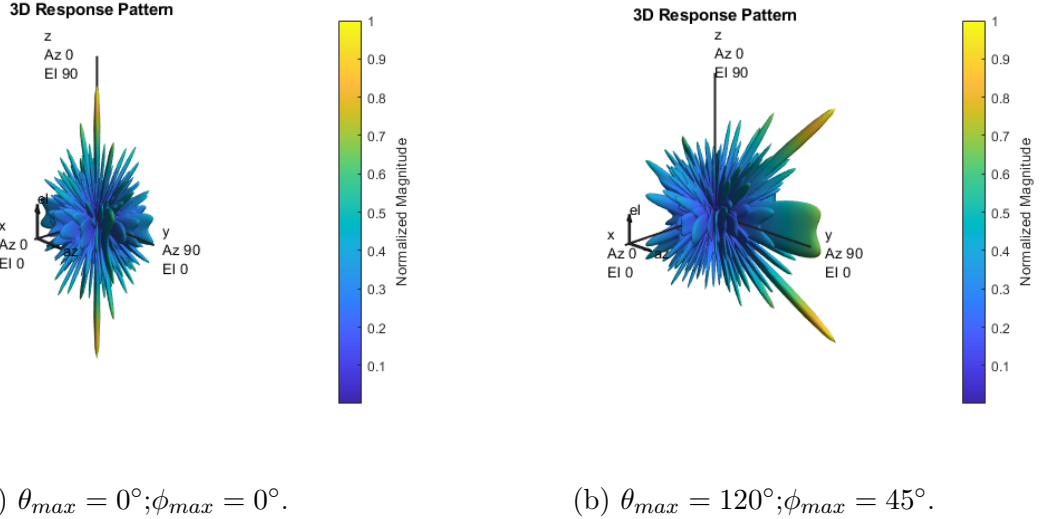


Figure 4.3: Radiation Pattern components of a Distributed Planar Array.

As it is possible to analyse comparing Figs. 4.3a and 4.3b, the sides lobes keep existing and are similar between them. However, the main beam is clearly dislocated in another direction. Before aiming to the center, this is now pointing in the desired direction.

4.3 Position-based distributed beamforming: system model and simulation testbed

In this study, we will delve deeper into distributed beamforming for WSNs, using the knowledge of sensor positions to determine the precoding beamforming factors for each sensor node. The simulation testbed will also assess the impact of inaccurate position information or lack of achievement.

A two-dimensional illustration of the scenario environment implemented in the simulation testbed is presented in Fig. 4.4. The system consists of numerous sensor nodes, depicted as temperature sensors, for representational purposes. These network nodes are assumed to be co-planar, signifying they reside within a single plane. All the sensors communicate with a single Central Processing Unit (CPU) or an equivalent processing unit responsible for determining their absolute positions within the testbed. The designated receiver for this investigation is a drone tasked with acquiring signals transmitted by the deployed sensors. It is important to note that communication between the sensor nodes and the CPU is not explicitly modelled in this study; the focus lies on the communication between the sensor nodes and the drone receiver.

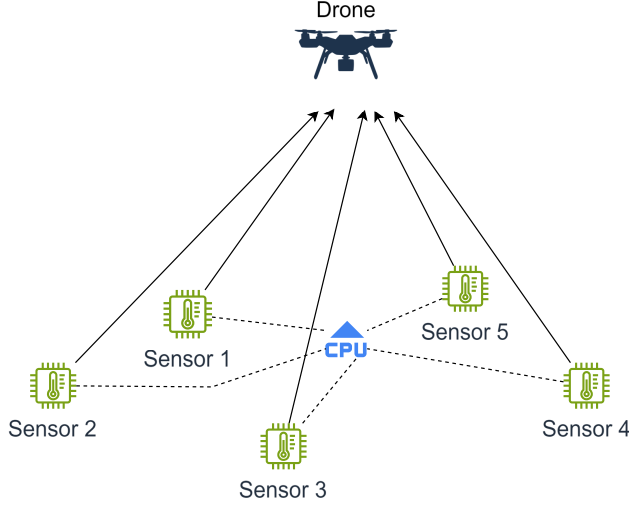


Figure 4.4: Schematic of Testbed.

A deeper analysis of previously discussed parameters and scenarios will be conducted using the developed simulation testbed. We will evaluate various metrics related to beamforming performance, including array factor and signal strength. The testbed will also be employed to analyse the influence of factors such as the number of nodes, wavelength on beamforming effectiveness and different performances for WSNs in the near-field and far-field. The code of the testbed is presented in [5].

We will first present near-field scenarios, starting with the ideal scenario and its corresponding received signal at the BS to facilitate the beamforming analysis. This will serve as a benchmark for understanding system limitations as we compare the ideal scenario to scenarios with inaccurate information about the sensors' position.

4.4 Near-Field Distributed Beamforming Ideal Scenario

The testbed developed simulates a square field with a side length of 10 wavelengths (λ). Nodes are randomly distributed within this field and transmit signals to a BS, assumed as a drone, located at the center with a height of 20λ having a minimum height of 1m and a maximum height of 10m, when operating at the frequencies of 6GHz and 600MHz, respectively. Fig. 4.5 is an example of a possible field.

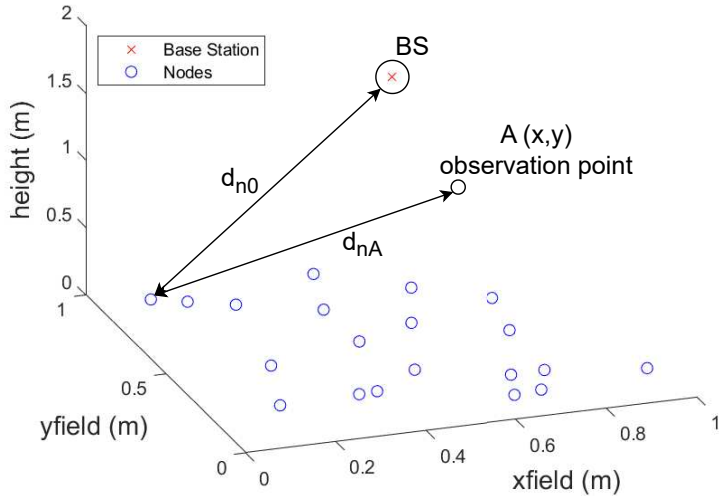


Figure 4.5: Distributed WSN with 20 nodes randomly placed.

Since the sensors are at different distances, R_n , from the BS, and considering that the speed propagation is equal to the speed of light, c , signals will arrive at the receiver at different timestamps. We can calculate the appropriate time delay for each signal to ensure its arrival at the receiver according to

$$t_n = \frac{R_n}{c}. \quad (4.6)$$

where the obtained results are shown in Fig. 4.6, where it is assumed for a matter of easy understanding that each sensor sends a pure sinusoidal signal at the carrier frequency. In Fig. 4.6 and the ones that follow, until further notice, whenever temporal results are shown, we have considered simulation frequency, f_c , as 3GHz.

As observed in Fig. 4.6, the received signals exhibit a substantial mismatch, indicating a misalignment between the desired signal phases and the actual received phases. This mismatch can lead to performance degradation in communication systems. To address this challenge, precoding techniques are often employed to manipulate the phases of the transmitted signals at the source [31]. By strategically adjusting the phases, precoding aims to improve the alignment between the transmitted and received signals, thereby mitigating the observed mismatch.

Building upon the foundational concepts presented in [24], (4.7) is derived. This equation likely describes the mathematical relationship between the precoding matrix and the achieved

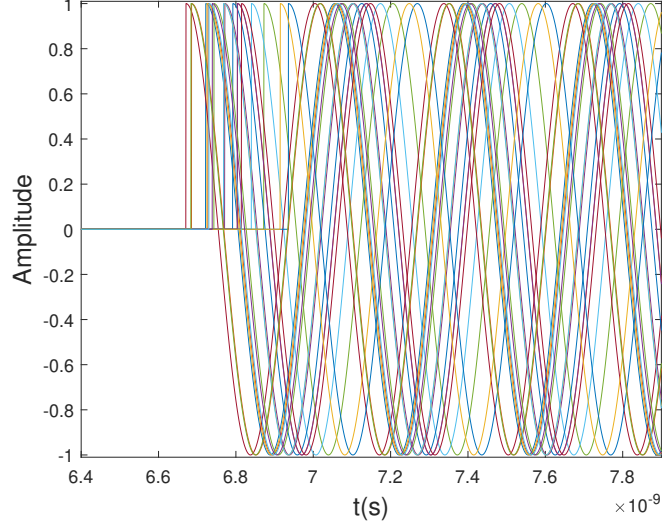


Figure 4.6: Time of arrival of each signal, for scenario in Fig. 4.5 at frequency $f_c = 3\text{GHz}$.

phase adjustments.

$$\Psi_n = \frac{2\pi}{\lambda} (R_{max} - R_n). \quad (4.7)$$

where R_{max} represents the greatest distance between every node and the BS. This maximum distance serves as a reference, assigning a phase zero to the sensor at that distance. By combining (4.6) and (4.7), it is possible to achieve an ideal constructive signal within the system, as shown in Fig. 4.7.

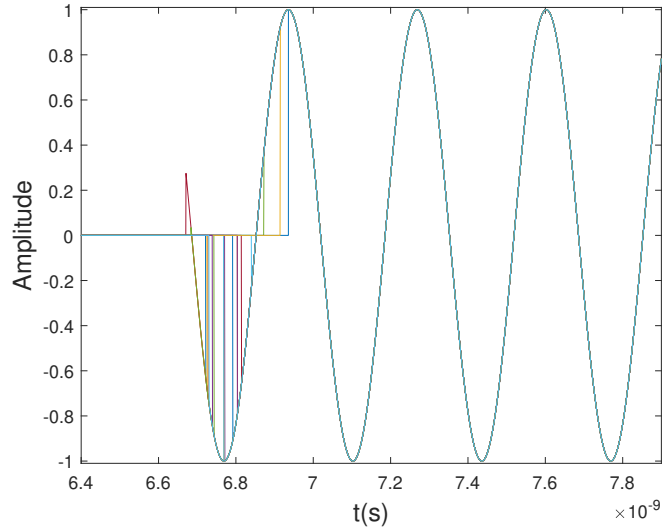


Figure 4.7: Phase-compensated signals at the receiver.

Now, the phases are correctly adjusted, and constructive beamforming is achieved. The summation of these temporally aligned signals then yields the desired received signal shown

in Fig. 4.8.

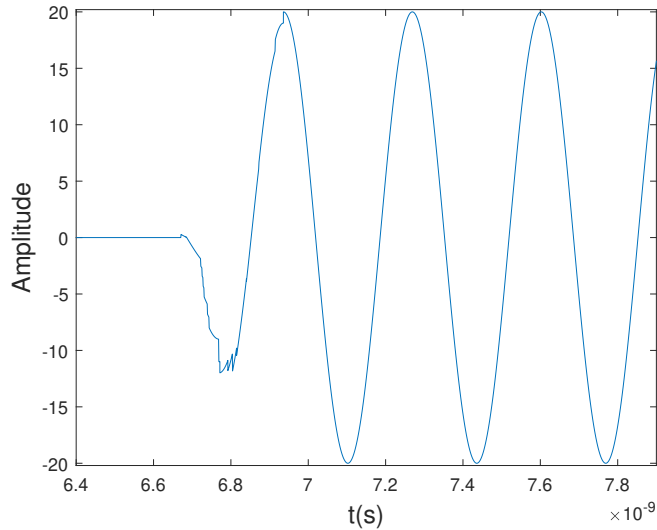


Figure 4.8: Received ideal signal for a WSN with 20 nodes randomly placed nodes.

Due to the unitary amplitude of each node, the concept of amplitude gain becomes less relevant in this context. However, considering the power is proportional to the square of the amplitude, coherent beamforming offers a potential power gain of N^2 . This gain arises from the constructive combination of the signals at the intended receiver. This gain is also explained using the (4.8), as in [19],

$$AF(x, y) = \sum_{n=1}^N e^{j\frac{2\pi}{\lambda}(d_{nA} - d_{n0})} \quad (4.8)$$

that computed the AF at an observation point $A \equiv (x, y)$, disregarding sensors' signal attenuations due to distance travelled, only considering phase difference toward signals at BS reference point, as represented in Fig. 4.5, toward beamforming is designed.

In (4.8), d_{nA} and d_{n0} are, respectively, the distance from the sensor n to the observation point, A and BS. We can observe that by setting the observation point A to be BS, then $d_{nA} = d_{n0}$, yielding an amplitude gain of N at A , and a power gain of N^2 , as mentioned before. However, this gain can only be observed in the far field where distance d_{nA} can be considered equal for all the sensors.

In the near field, one factor that can't be ignored is the propagation loss present in every wireless communication system. Thus, the received power is given by Friis' formula [26].

$$P_{BS_n} = P_n G_n G_{BS} \left(\frac{\lambda}{4\pi R_n} \right)^2 \quad (4.9)$$

where P_n and P_{BS_n} are the power transmitted and received at BS for sensor n, respectively, in Watts (W), G_{BS} and G_n are the receiver and transmitter directivity gains, respectively.

For fixed antenna gains, the propagation loss can be given by (4.10):

$$PL_n = \frac{P_n}{P_{BS_n}}. \quad (4.10)$$

Fig. 4.9 illustrates the path loss experienced by each sensor in the example system, obtained at the frequency of 3GHz.

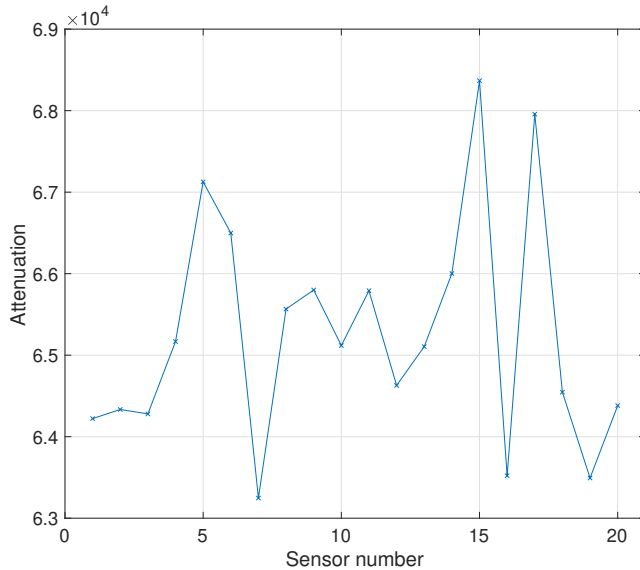


Figure 4.9: Signal attenuation of each sensor for the scenario of Fig. 4.5, when the BS (drone) is at a height of 20λ .

We obtain a more realistic representation of the received signal strengths by applying path loss to each sensor's signal. Fig. 4.10 depicts the received signals after incorporating the path losses.

The substantial path losses, on the order of 10^4 , lead to a markedly weakened received signal amplitude, as anticipated. Despite these significant path losses, the signal depicted in Fig. 4.10 represents a realistic and achievable outcome for a system like ours under these propagation conditions. Note that according to (4.9), and considering our scenario where the BS is at 20λ height, the minimum power attenuation suffer by each sensor's signal is $(\frac{4\pi \times 20\lambda}{\lambda})^2 = (80\pi)^2$. Thus, an upper-bound on signals amplitude in Fig. 4.10 is $\frac{N}{80\pi} = \frac{20}{80\pi} \approx 0.0796$, which is consistent with the results obtained.

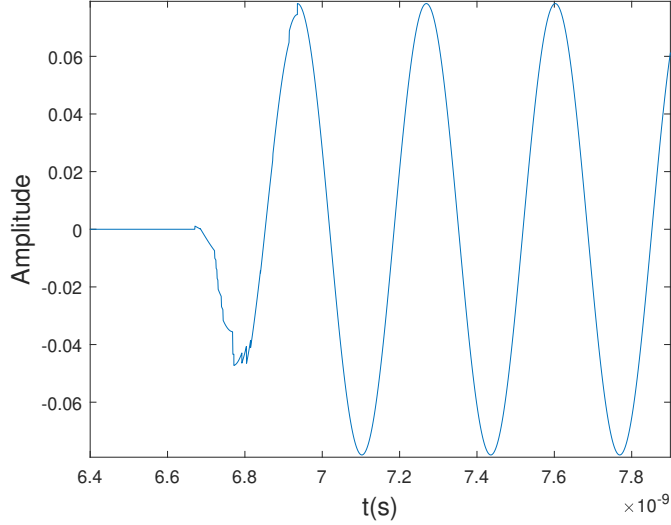


Figure 4.10: Received attenuated signal for a WSN with 20 nodes randomly placed nodes.

4.5 Impact of Sensor Position Error in Near-Field Distributed Beamforming

Building upon the ideal scenario presented in Section 4.4, this section explores the impact of sensor position errors in real-world deployments. We will introduce controlled errors to the sensor positions within the testbed, allowing us to analyse the effects of these errors on the final received signal. An illustration of the testbed environment for sensor position error employed in these simulations is presented in Fig. 4.11.

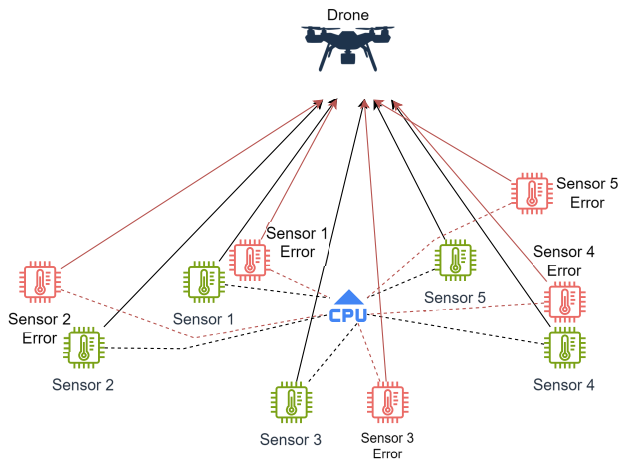


Figure 4.11: Schematic of Testbed Sensors Position Error.

To investigate the effects of sensor position errors, we applied random Gaussian errors with a variance of 0.2λ in all axes to the sensor positions within the field depicted in Fig. 4.5.

This process resulted in sensor distributions similar to those shown in Fig. 4.12.

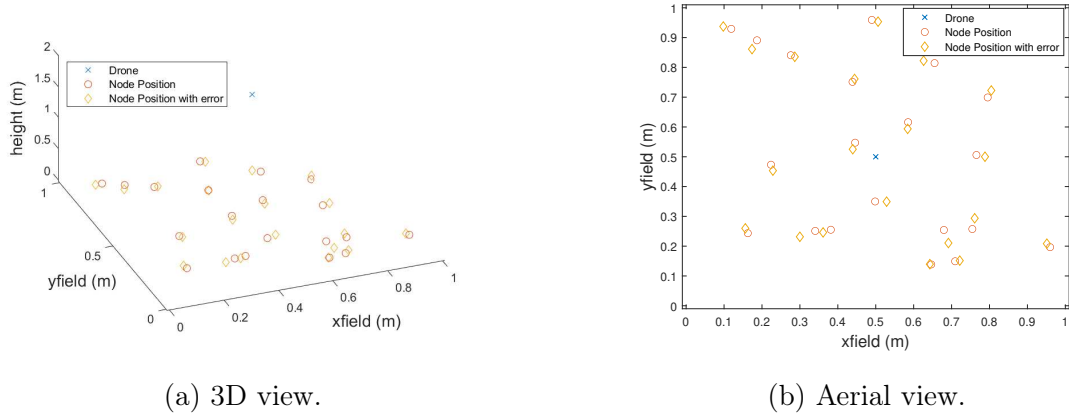


Figure 4.12: Distributed WSN with 20 nodes randomly placed with node position error.

Therefore, a simulation was conducted to analyse the impact of sensor position errors on the received signal. The results are presented in Fig. 4.13.

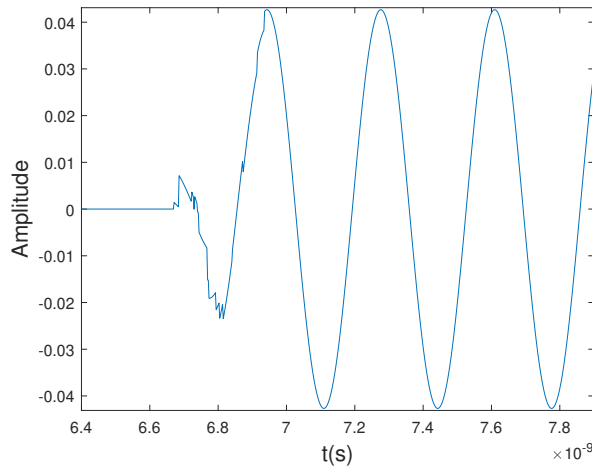


Figure 4.13: Distributed WSN with 20 nodes randomly placed with position error.

By comparing the results in Fig. 4.13 with those in Fig. 4.10, we observe a significant reduction in the received signal power. In this scenario, with sensor position errors, the signal amplitude is approximately half compared to the ideal case.

4.5.1 Sensor Position Error and Signal Degradation

Having established the significant impact of sensor position errors on signal quality, we now investigate the system's behaviour under these errors. This analysis will determine the resilience of this wireless communication system to such imprecisions.

We conducted various tests with different error variances to evaluate the system's resilience to position errors. For each error variance, 300 simulations were made using the scenario shown in Fig. 4.5 as a base. The error variances ranged from 0.05λ to 0.5λ in increments of 0.025λ . The results, presented in Fig. 4.14, were obtained by calculating the ratio of the maximum received signal amplitude, with sensors' position errors, to the maximum amplitude in the ideal scenario, i.e. exact knowledge of sensor position ,obtaining the boxplots using a MATLAB Toolbox [13].

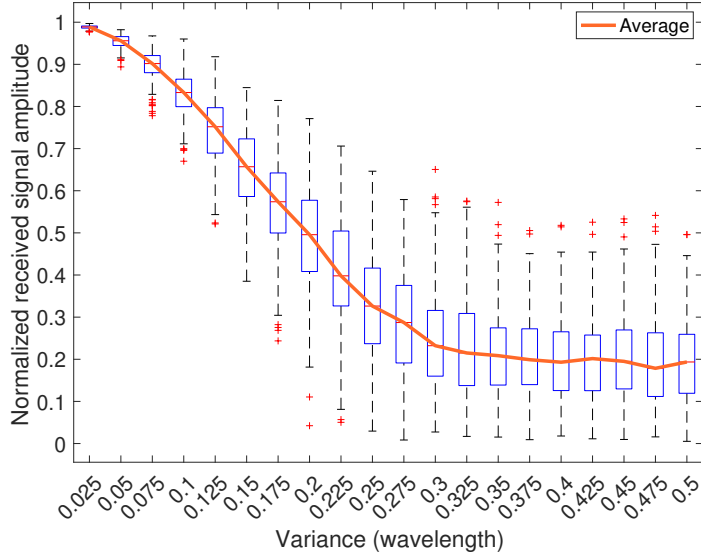


Figure 4.14: Normalized amplitude boxplot of distributed WSN with 20 nodes randomly placed with position error.

Figure 4.14 depicts the degradation of the received signal strength as the sensors' position error variance increases. A crucial aspect of this analysis is determining the maximum acceptable position error variance. We propose a threshold for the error variance of 0.175λ based on the combined analysis of the mean and boxplot distribution. This threshold corresponds to the last point where the signal exhibits a high probability of maintaining an amplitude exceeding half the original signal's amplitude level. We can also observe from Fig. 4.14 that for an error variance superior to approximately 0.4λ the received maximum amplitude stabilizes at a minimum of approximately 0.19% of the ideal received signal.

Despite this constant average, some changes in the 25% quartiles intervals are noticeable. The reduction in these quartiles indicates a possible convergence of the signal value towards the average obtained.

4.6 Impact of Base Station Position Error in Near-Field Distributed Beamforming

Beyond sensor position errors, receiver position inaccuracies can also significantly affect signal processing and localization performance. This section will investigate the influence of controlled errors introduced into the drone's position within the testbed environment. By maintaining known sensor positions and isolating the receiver position error as the sole variable, we systematically aim to analyse its impact on the received signal characteristics. An illustration of the testbed environment for drone position error employed in these simulations is presented in Fig. 4.15.

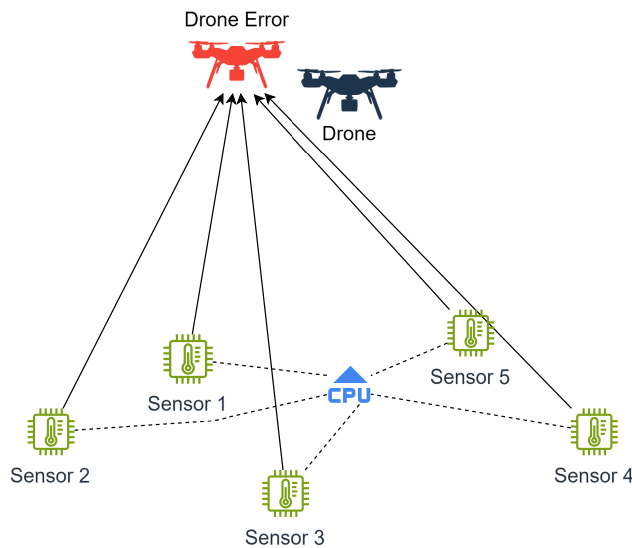
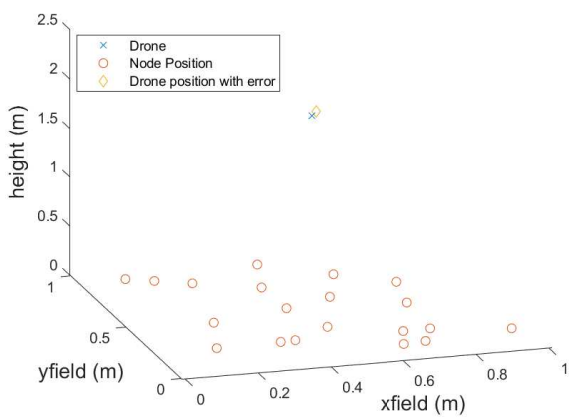
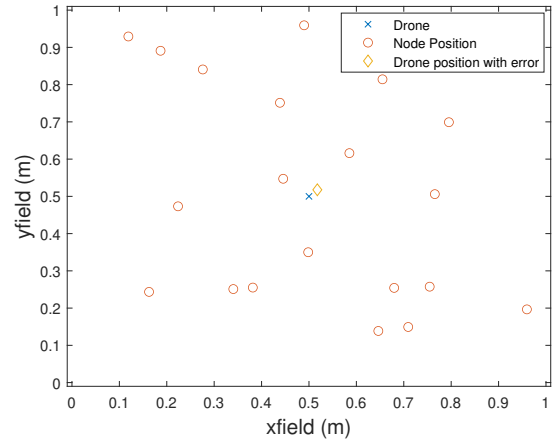


Figure 4.15: Schematic of Testbed Drone Position Error.

In the same way, as done in section 4.5, to investigate the effects of drone position errors, we applied random Gaussian errors with a variance of 0.2λ to the base station position, equal in every axis, being the field depicted in Fig. 4.16. Figs. 4.16a and 4.16b are shown the 3D view and the aerial view of the system, respectively.



(a) 3D view.



(b) Aerial view.

Figure 4.16: Distributed WSN with 20 nodes randomly placed with drone position error.

As this section utilizes the identical system configuration detailed in Section 4.4, the sensor propagation losses remain consistent with those presented in Fig. 4.9. This continuity in the system setup eliminates the need for redundant characterization of propagation losses.

Initially simulations investigating the impact of controlled receiver position errors revealed a greater tolerance for this type than sensor position errors, suggesting that the system to be less sensitive to variations in receiver location within a specific range. To quantify this tolerance, the simulations were executed with varying degrees of receiver position error, ranging from 0.025λ to 3.975λ in increments of 0.05λ , with results being presented in Fig. 4.17 and 4.18.

The objective is to present the effects of controlled receiver position errors on the maximum received signal amplitude. The variance in wavelength is depicted across the x-axis. The y-axis represents the normalized signal amplitude. To accommodate a large number of test cases, the boxplot is divided into two parts: Fig. 4.17 illustrates the results for errors ranging from 0.025λ to 2.975λ , while Fig. 4.18 shows the results for errors between 3.025λ and 3.975λ .

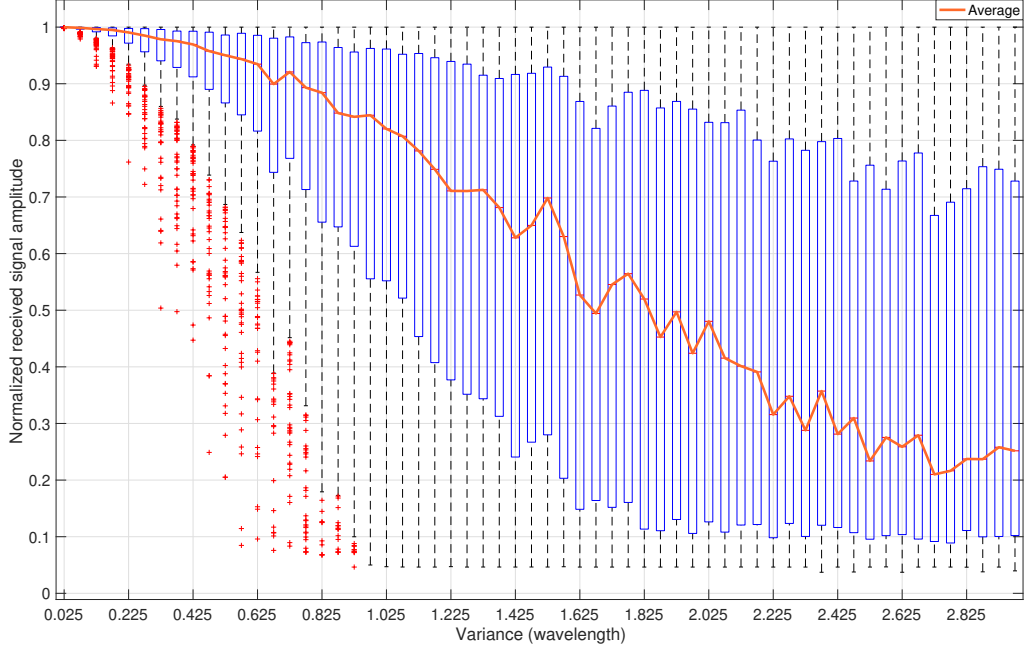


Figure 4.17: Normalized amplitude boxplot of distributed WSN with 20 nodes randomly placed with position error in the receiver 0.025λ to 2.975λ .

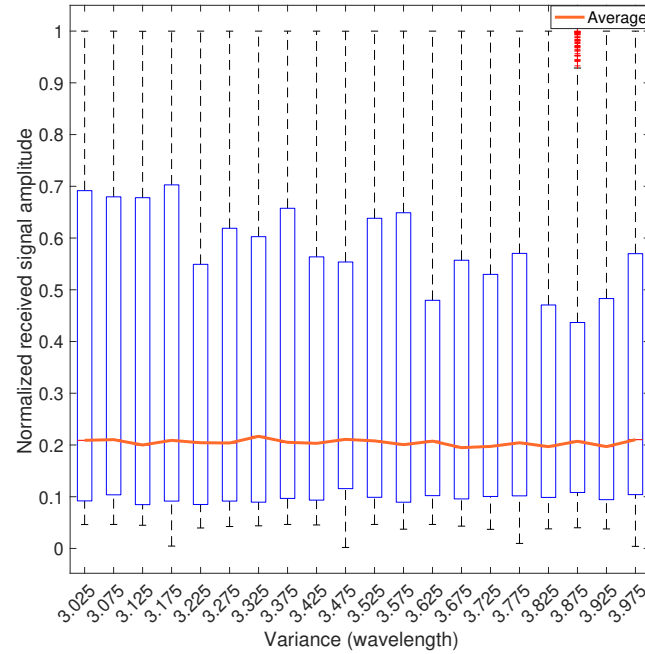


Figure 4.18: Normalized amplitude boxplot of distributed WSN with 20 nodes randomly placed with position error in the receiver 3.025λ to 3.975λ .

As illustrated in Fig. 4.17, the signal degradation is negligible within the range of 0.025λ to 0.325λ . Conversely, analyzing Fig. 4.18 reveals that the normalized mean of the received

signal amplitude remains relatively constant and very low throughout the studied error range (3.025λ to 3.975λ).

The analysis of the mean values obtained from the simulations suggests that signal degradation surpasses half amplitude in most scenarios when the drone position error exceeds 1.75λ . This implies a significant decline in signal quality beyond our threshold.

It can also be observed that for a drone position error variance below 1.025λ , only 20% reduction in the average amplitude is observed, though the variance is indeed very high, as is evidenced by the large length of the 25% quartile intervals, and that indeed error on estimating the correct position of the drone may indeed affect seriously the effectiveness of the distributed beamforming.

Fig. 4.18 also shows that similarly to what was observed for the case of unaccurate knowledge of sensors' position, that received normalized amplitude stabilizes at a minimum of 0.2.

4.7 Receiver Position Impact in Signal Quality in Near-Field Scenarios

For analytical tractability, the drone position was previously fixed at the center of the testbed. However, real-world scenarios necessitate investigating the influence of receiver location on the received signal. This section presents the results of simulations conducted to analyse the significance of receiver position in affecting the received signal quality.

The simulations investigating the impact of receiver position adopted a testbed environment modelled as a square field with dimensions of 10λ by 10λ . The field was discretized into a grid of smaller spaces to systematically evaluate the signal response across various locations. The drone's position was then iteratively placed at the center of each grid space within the testbed. Fig. 4.19 illustrates an example of the discretized field with a grid resolution of 25×25 spaces, resulting in 625 possible drone positions for analysis.

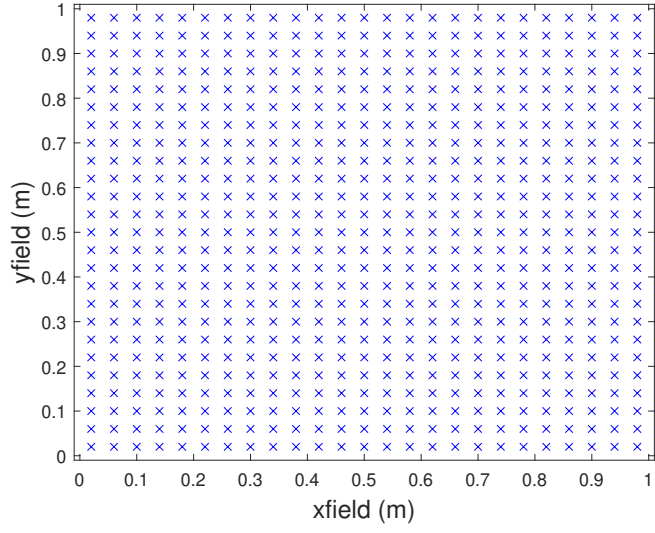


Figure 4.19: All drone possible positions in a 25×25 field.

As previously established, WSN topology is a critical factor influencing various system aspects, including optimal drone positioning for signal acquisition. Four unique random WSN deployments were generated within the testbed environment to investigate the impact of topology on the drone's optimal location. These deployments are visualized in Fig. 4.20.

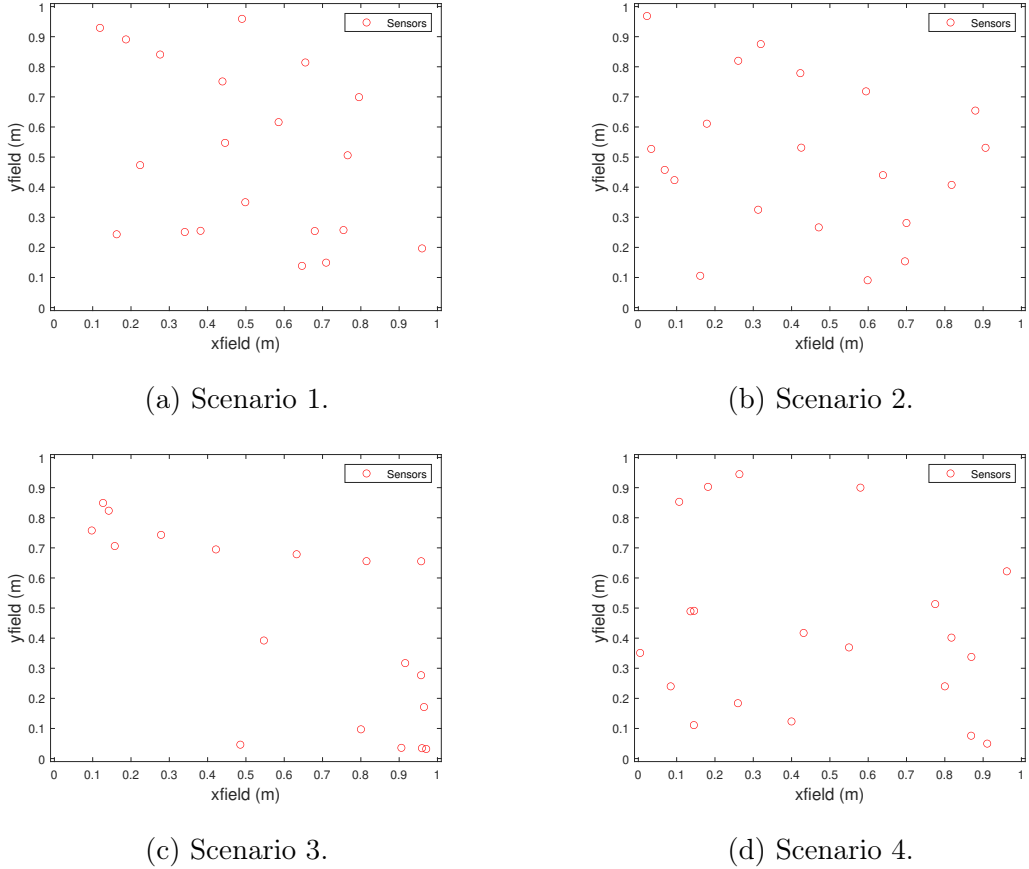


Figure 4.20: The 4 scenario used to test drone optimum position.

Each of the four randomly generated WSN deployments, as illustrated in Fig. 4.20, comprised 20 sensors arranged in distinct spatial configurations. To evaluate the influence of topology on received signal strength, the simulations captured the maximum signal amplitude achievable for each possible drone position within the testbed. Subsequently, these amplitudes were normalized relative to the maximum amplitude observed across all positions. The resulting normalized signal strength distributions for each WSN topology are depicted as colormaps in Fig. 4.21.

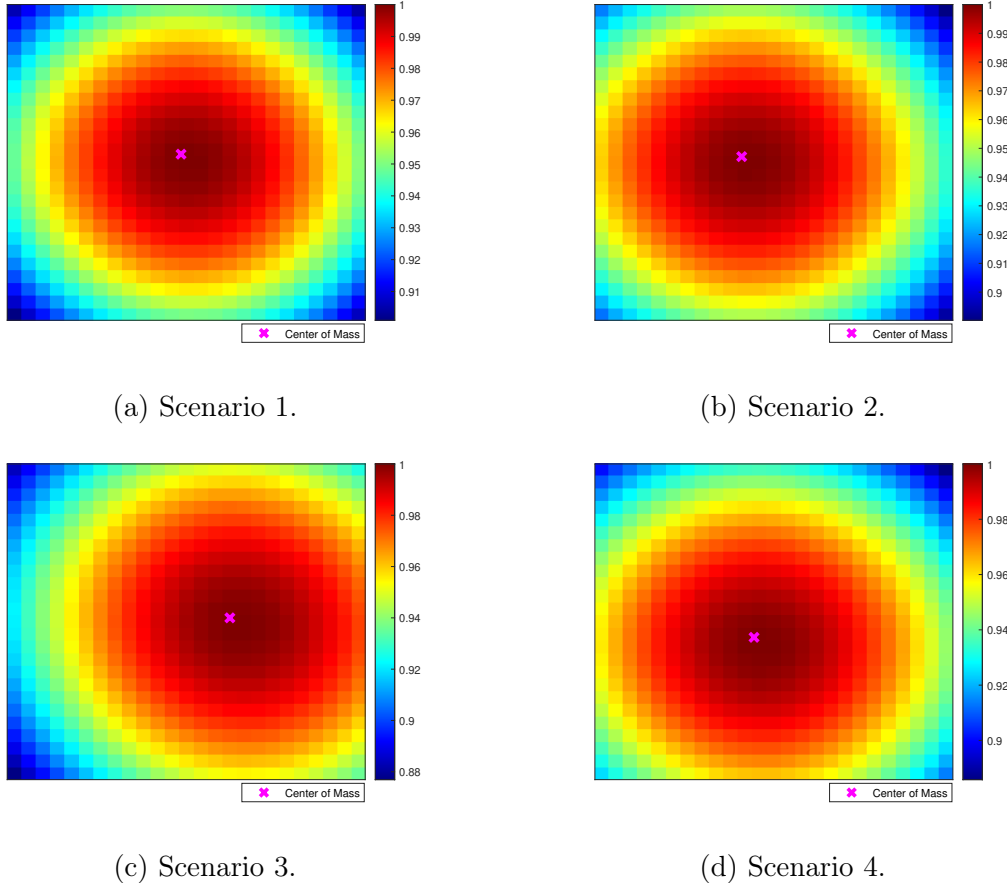


Figure 4.21: Colormaps for the 4 scenario studied.

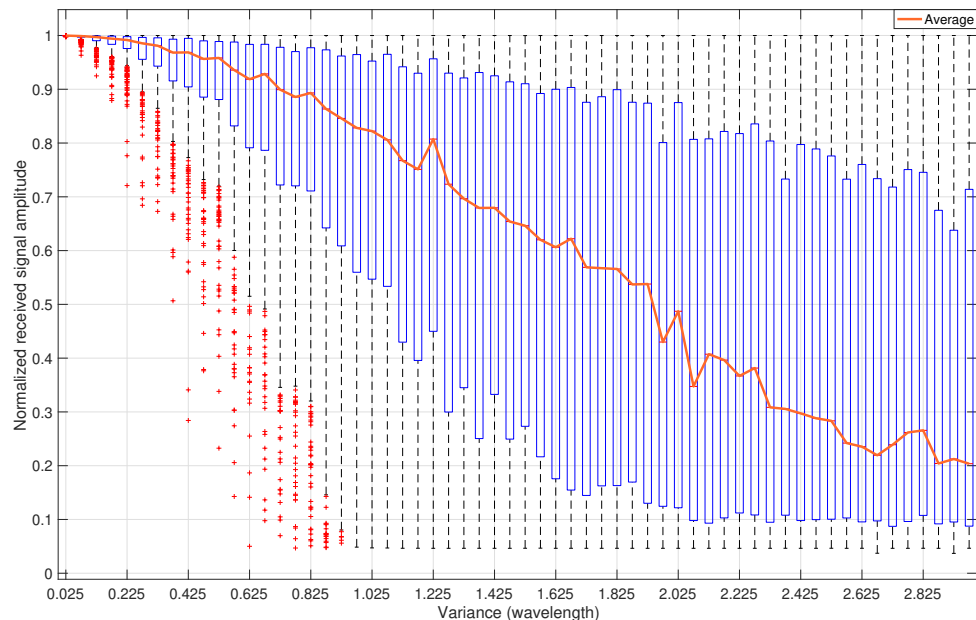
The analysis of the colormaps in Fig. 4.21 reveals that the maximum normalized signal amplitude is consistently achieved at the center of mass, centroid, of the sensor distribution within each WSN topology. As indicated by the colorbars, while there is a distinct optimal position and centre of mass, a significant portion of the testbed area exhibits near-optimal signal strength values. This implies that some degree of flexibility may be possible when selecting the drone's positioning for signal acquisition, particularly in scenarios where the exact center of mass might be impractical.

More importantly, by combining the given results with the ones from Section 4.5 and 4.6,

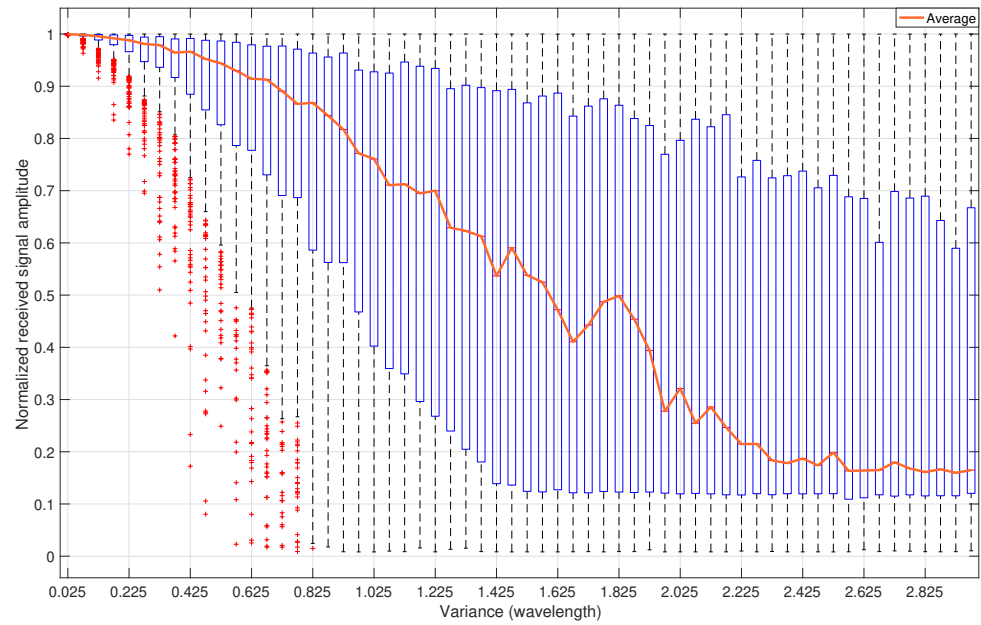
that while the position within the area where most sensors are distributed is not a concern, the exact coordinates of the drone are important toward efficient distributed beamforming, and obtain maximum aggregate gain.

Having established the center of mass of the WSN deployment as the optimal drone location for signal acquisition, as observed in Fig. 4.21, this section investigates the resulting signal degradation under this optimized positioning scenario. The simulations replicate the tests conducted previously in Figs. 4.17 and 4.18 to assess if the degradation patterns remain similar when the drone is positioned at the optimal location. Fig. 4.22 and 4.23 show the results obtained.

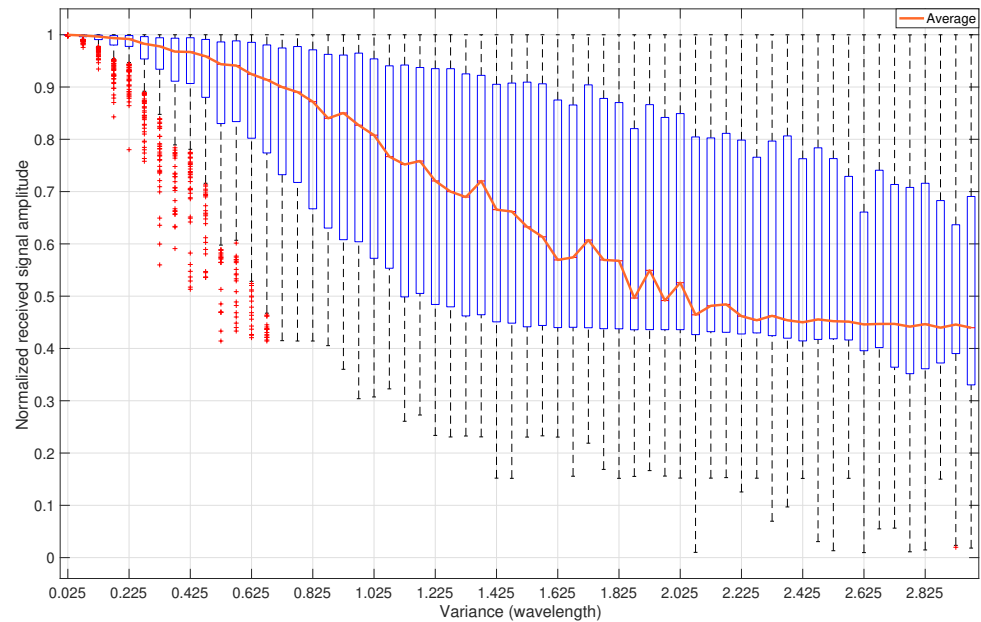
This suggests that the fundamental characteristics of signal degradation remain consistent even when the receiver is placed at the optimal position. However, it is noteworthy that each WSN topology demonstrates a distinct sensitivity to position errors. For instance, Scenario 3 exhibits a higher received signal power average than other deployments. This can be attributed to a potentially larger optimal signal region within Scenario 3's spatial sensor configuration than the other WSN layouts. Another important factor that is also possible to notice is the length of the 25% quartile intervals. Besides the slower decrease of the received signal amplitude, when compared with the sensors' position error scenario, the boxes increase their size with the variance increase. This size increase means that the received signal power is less predictable, making it harder to control the system's behaviour.



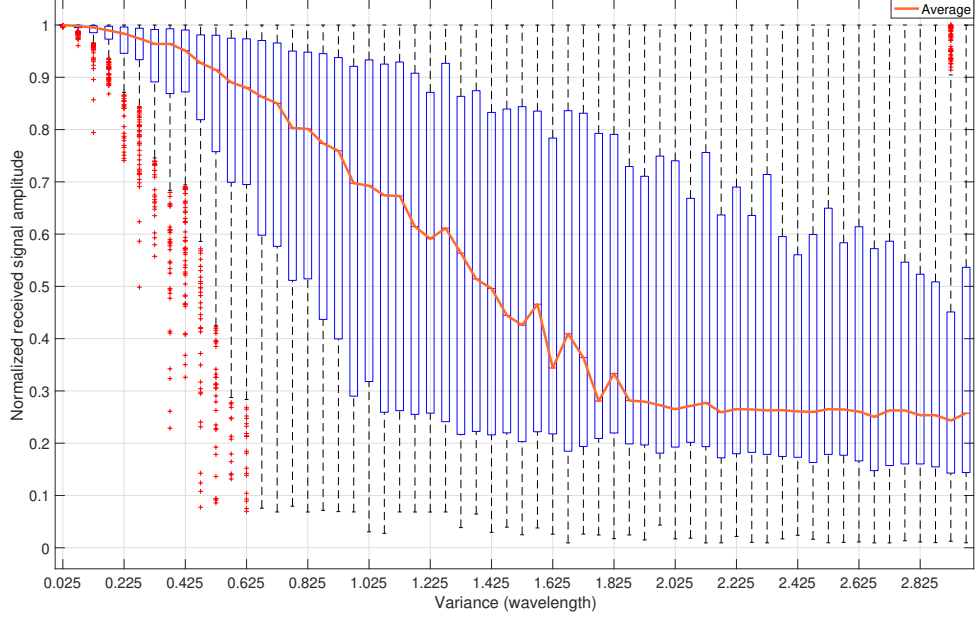
(a) Scenario 1.



(b) Scenario 2.



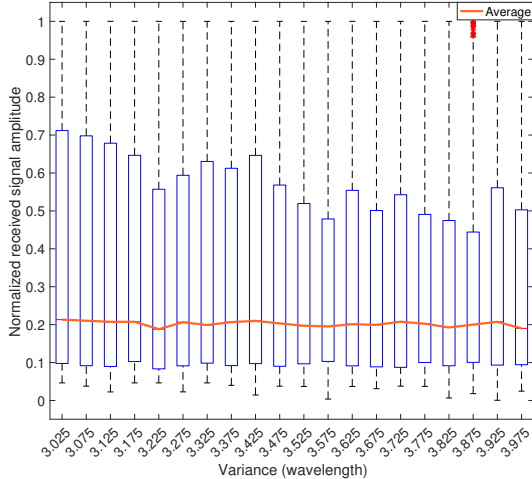
(c) Scenario 3.



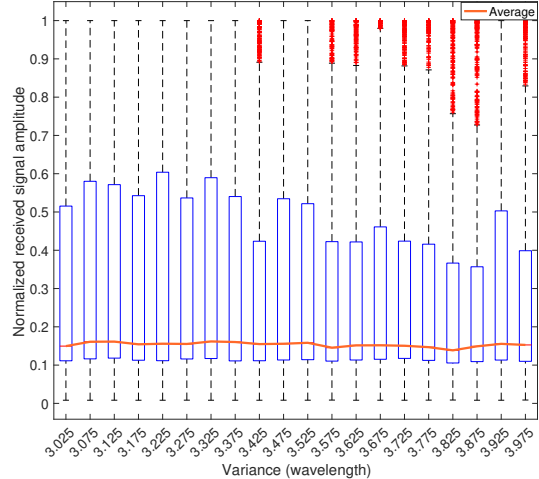
(d) Scenario 4.

Figure 4.22: Normalized amplitude boxplot of distributed WSN with 20 nodes randomly placed with position error in the receiver 0.025λ to 2.975λ .

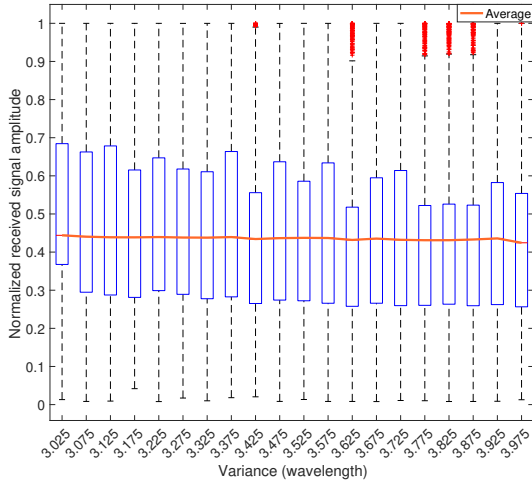
Figure 4.23 illustrates the behaviour of the system's received signal mean as a function of the BS' position error variance. It is possible to observe that for error variances exceeding 3λ , the mean of the received signal stabilizes. This is a noteworthy change compared to the previous observations, where the mean was always 20%. Now, it is possible to notice that the mean also depends on the network topology. Interestingly, the distribution of the received signal, as represented by the boxplots, also changes. The size of the boxes, representing the interquartile range, decreases for higher error variances. Additionally, the boxes appear to be shifting towards the overall mean value.



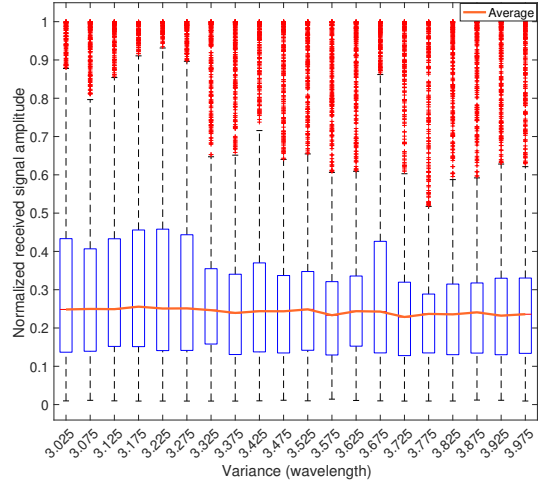
(a) Scenario 1.



(b) Scenario 2.



(c) Scenario 3.



(d) Scenario 4.

Figure 4.23: Normalized amplitude boxplot of distributed WSN with 20 nodes randomly placed with position error in the receiver 3.025λ to 3.975λ .

4.8 Impact of Received Power Adjustment in Near-Field Distributed Beamforming

Considering the low-power nature of the WSNs employed in this study, the transmitted power from each sensor is inherently limited. Therefore, toward reducing power consumption and extending the battery life of WSN nodes, it makes sense to adjust the transmitting power of sensor nodes toward achieving a minimum desirable received power at BS. This adjustment aims to compensate for potential variations in transmission power levels across different sensors. After the adjustments, the studies in Sections 4.5 and 4.6 will be repeated to

analyse and verify the system behaviour.

Leveraging the WSN depicted in Fig. 4.5, the limited transmission power of the sensors by implementing a power adjustment procedure. To achieve this, the propagation losses experienced by each sensor are first analysed. These propagation losses, likely visualised in Fig. 4.5, account for the signal attenuation that occurs as the signal travels from the sensor to the receiver. Defining the minimum required power per sensor at BS as P_{ref} corresponding to a "virtual" sensor node with transmitting power, P_t , at reference distance, d_{ref} , then for sensor n, transmitting at $P_{t_n} = P_t$ the appropriate power adjustment A_n^2 is

$$A_n^2 \left(\frac{4\pi d_n}{\lambda} \right)^2 = P_{ref} \Leftrightarrow A_n^2 \left(\frac{4\pi d_n}{\lambda} \right)^2 = \left(\frac{4\pi d_{ref}}{\lambda} \right)^2 \Leftrightarrow A_n^2 = \left(\frac{d_n}{d_{ref}} \right)^2 \quad (4.11)$$

The signal sent by each sensor n is thus adjusted as

$$s_{n_{adjust}} = A_n s_n. \quad (4.12)$$

With sensors' transmitted amplitudes being shown in Fig. 4.24 for the scenario of Fig. 4.5, considering as reference sensor the one farther away from the drone.

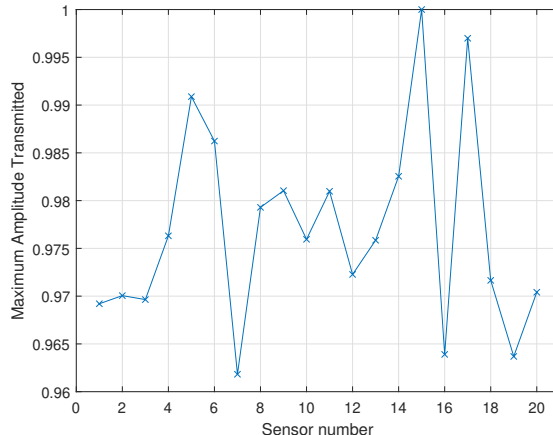


Figure 4.24: Transmission amplitude by each sensor.

With this information, we can calculate the average amplitude transmitted. This result is approximately 0.977 for this system, which means that the transmitted amplitude is 2.3% lower than the signal transmitted in the other scenarios studied above, where all the models were transmitting at maximum power. So, no efficiency gains were to be expected for these particular scenario of sensor distribution, since the differences between d_n and d_{ref} are small. Even though, to confirm the initial reasoning the same procedure on simulation was conducted.

Fig. 4.25 is similar to Fig. 4.7 by depicting the sensor signals after the application of the amplitude adjustments calculated in (4.11).

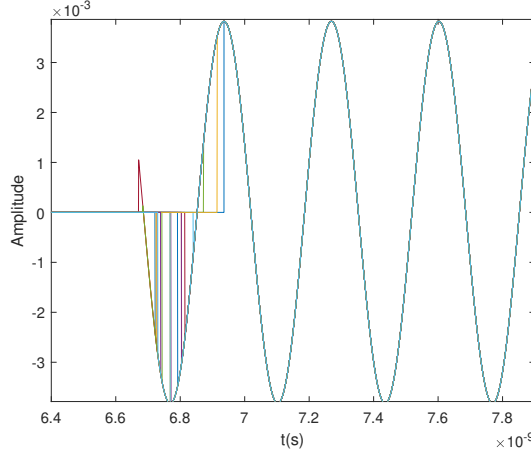


Figure 4.25: Received signals with amplitude adjusted.

The received signal after the adjustment, shown in Fig. 4.26, shows an amplitude 2.3% smaller than the amplitude when no adjustments are made. This suggests that the total received signal amplitude will reduce linearly with each individual received signal's mean of reduced amplitude.

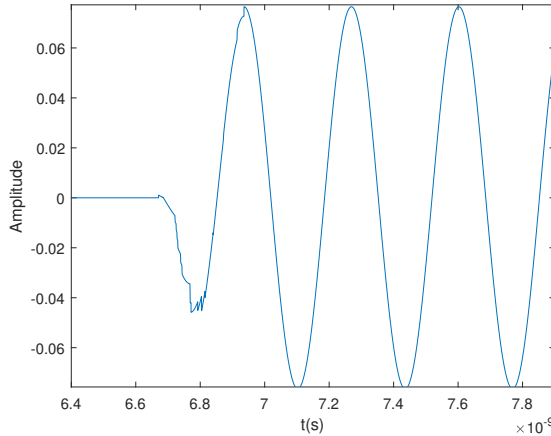
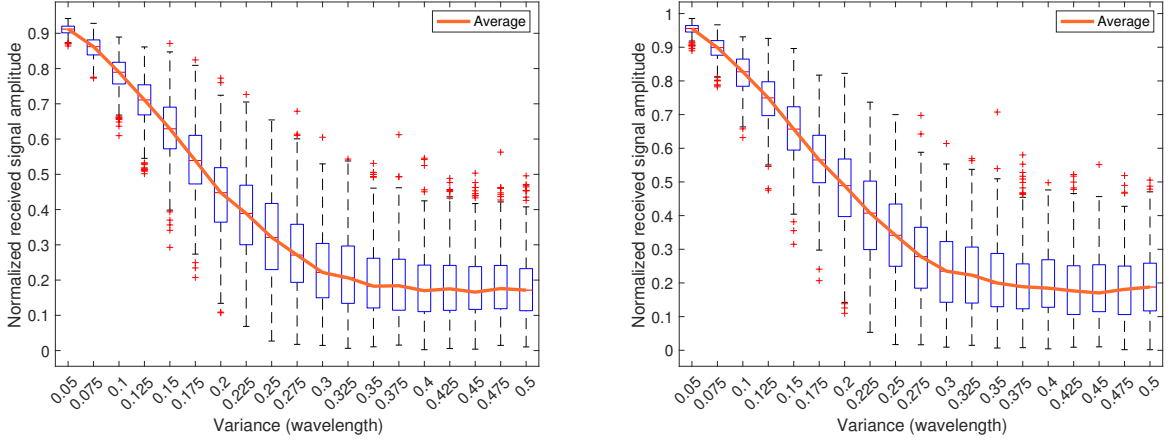


Figure 4.26: Total received signal with amplitude adjusted.

Having achieved power adjustment across the WSN, we can now analyse the effects of sensor position errors. Fig. 4.27 depicts a boxplot summarizing the results obtained from test cases involving sensor position errors ranging from 0.05λ to 0.5λ . Fig. 4.27a shows the received signal after the adjustment with sensors' position error normalized by the ideal received signal before the adjustment. Fig. 4.27b shows the received signal after the adjustment with sensors' position error normalized by the ideal received signal after the adjustment.



(a) Normalized by the ideal signal without adjustment.
(b) Normalized by the ideal signal with adjustment.

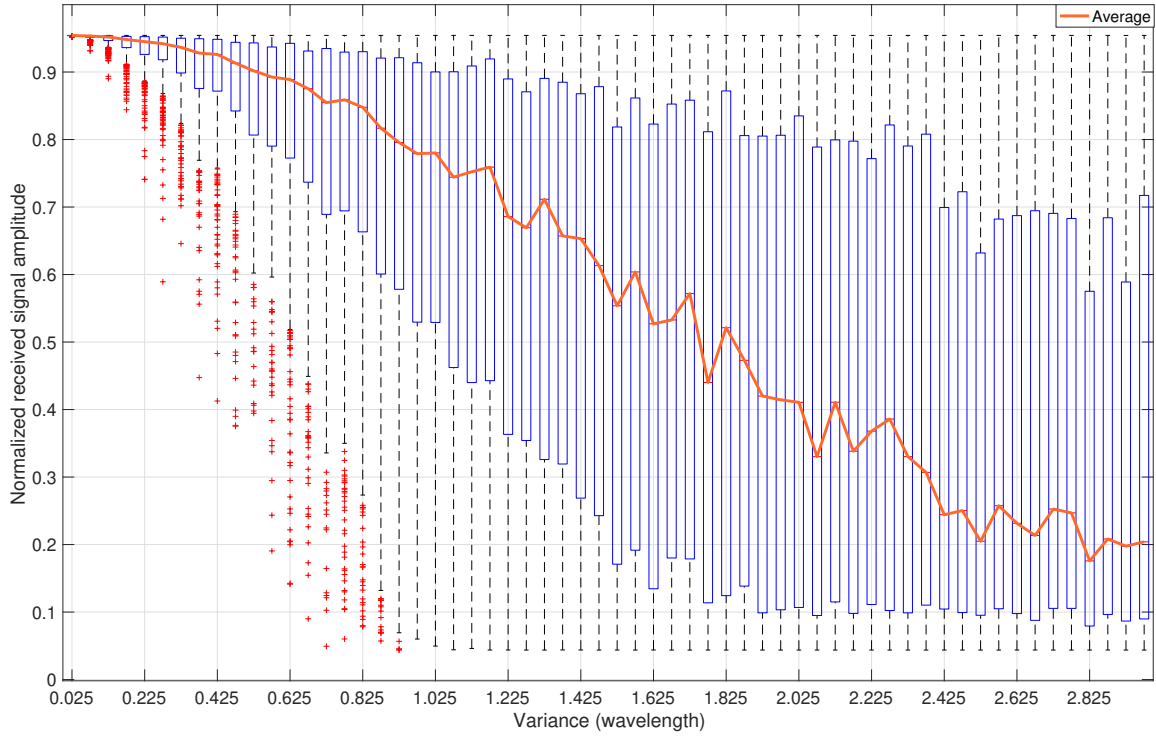
Figure 4.27: Normalized amplitude boxplot of distributed WSN with 20 nodes randomly placed with the sensors' position error.

Analyzing the results obtained in Fig. 4.27, the results suggest that a sensor position error variance of approximately 0.175λ leads to a signal strength decrease of around 3%. This value corresponds to the last point on the graph before the average falls below 0.5, indicating a potential threshold for significant signal degradation due to sensor position uncertainties.

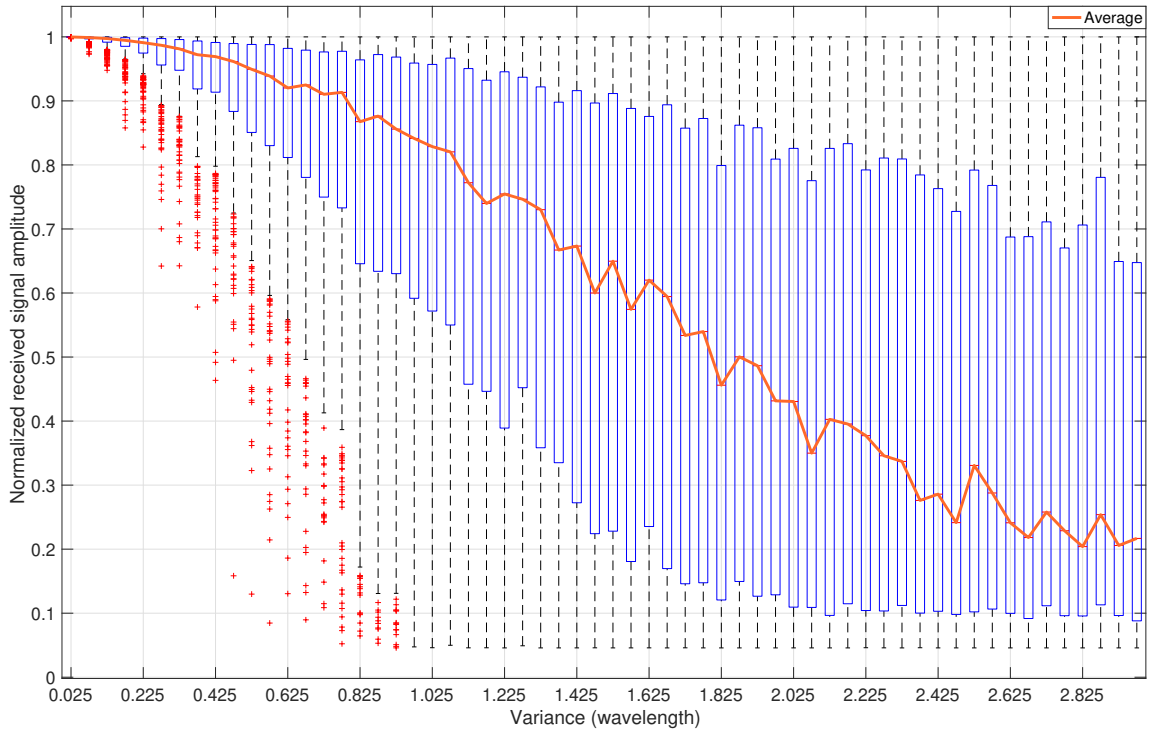
Fig. 4.28 depicts a boxplot summarizing the results obtained from test cases involving drone position errors ranging from 0.025λ to 3λ . Fig. 4.28a shows the received signal after the adjustment with sensors' position error normalized by the ideal received signal before the adjustment. Fig. 4.28b shows the received signal after the adjustment with sensors' position error normalized by the ideal received signal after the adjustment.

In this case, degradations increase with the variance increase being approximately 6% at 1.725λ .

While amplitude adjustment offers a potential method for mitigating signal strength variations in wireless sensor networks, it may not be the most advantageous technique for the scenario investigated in this chapter. The analysis revealed that the reduction in signal amplitude from individual sensors might not be significant enough to fully compensate for the potential errors introduced during the adjustment process. These errors could arise from factors like imperfect calibration or environmental noise.



(a) Normalized by the ideal signal without adjustment.



(b) Normalized by the ideal signal with adjustment.

Figure 4.28: Normalized amplitude boxplot of distributed WSN with 20 nodes randomly placed with the drone's position error with adjusted amplitude.

To conclude this section, besides the possible benefits of amplitude adjustment, in the case studied, this technique does not significantly impact the power consumption of the WSN. However, power consumption may be reduced significantly for networks where the distance differences are more considerable than those used in this scenario.

4.9 Far-Field Distributed Beamforming Ideal Scenario

Following the investigation of a WSN operating in the near-field relative to the receiver position, this work will extend the analysis to the far-field region. To achieve this, the system was developed based on the schematic depicted in Fig. 4.4 and the principles outlined in (2.1). To ensure the WSN operates within the far-field for a practical drone flight height, a square field with dimensions of $10\lambda \times 10\lambda$ was chosen. Additionally, the operating frequency was set to 6GHz. With these parameters, an appropriate drone height of 10 meters was set, as shown in Fig. 4.29.

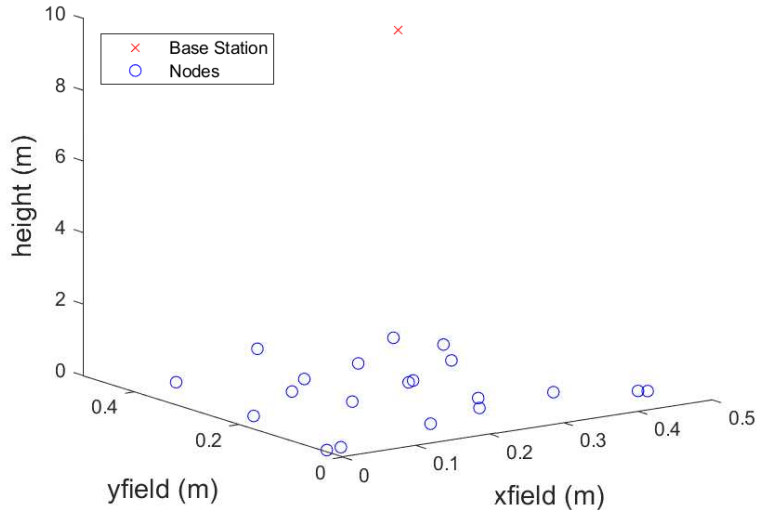


Figure 4.29: Distributed WSN with 20 nodes randomly placed.

Within the far-field region, as established in the previous section, it becomes possible to determine the array factor for our sensor network. The array factor describes the radiation pattern of the antenna array, essentially indicating the direction of maximum power transmission. As expected, our analysis reveals that the maximum power is directed towards the drone's location.

To visualize this radiation pattern, we utilized the MATLAB App Sensor Array Analyzer [12]. The resulting beamforming plot is depicted in Fig. 4.30.

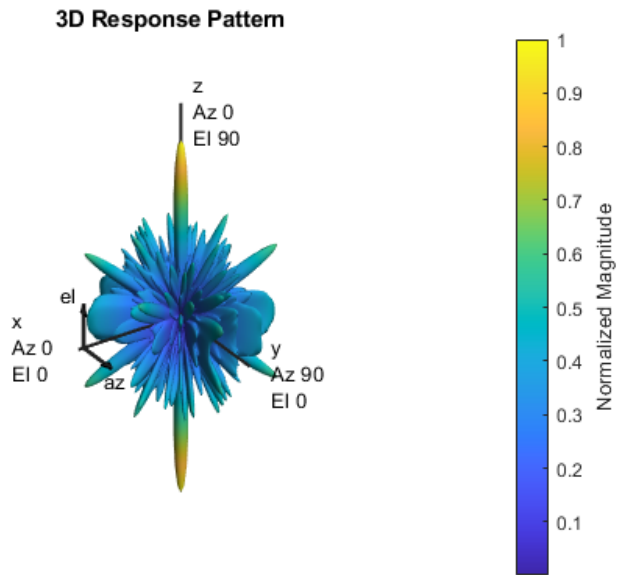


Figure 4.30: Field beampattern.

The distance between all sensors and the receiver is practically the same in the far-field. This makes the losses similar for every sensor, as shown in Fig. 4.31

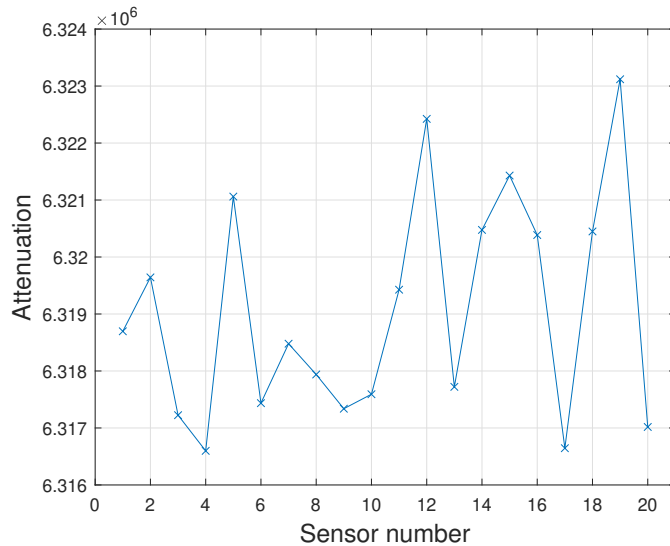


Figure 4.31: Signal attenuation of each sensor.

These similar distances also imply that the signal's travelling time is much similar for every sensor, as shown in Fig. 4.32.

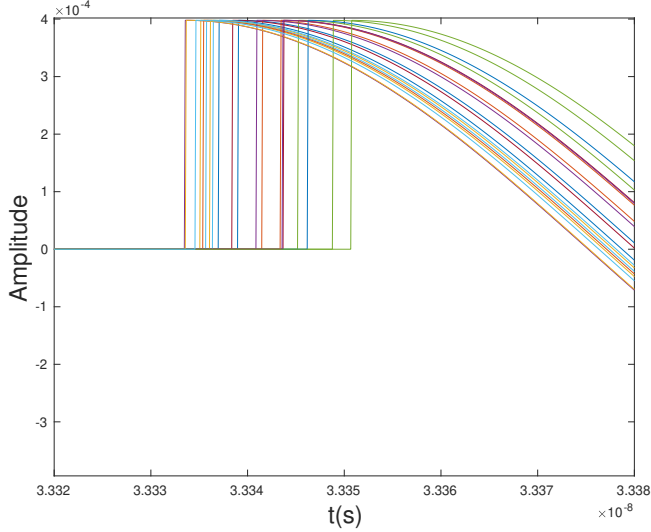


Figure 4.32: Time of arrival of each signal.

As mentioned before, in the far-field, some assumptions are made, such as the approximation of the array of sensors to a single point. Thus, to study the impact of this assumption, the phase was adjusted, as shown in Fig. 4.33, obtaining the ideal signal for this system.

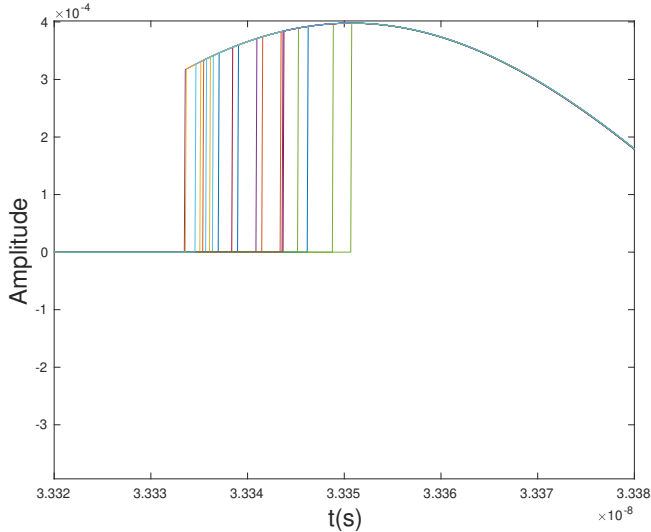


Figure 4.33: Phase-compensated signals at the receiver.

Dividing the maximum amplitudes from signals shown in Fig. 4.34, we obtain that, without adjusting the signals' phase, the signal amplitude is approximately 98%, or -0.18dB .

This means that the impact of phase adjustments on the received signal becomes negligible. The need for complex phase adjustments at the sensor level is eliminated, which is a significant advantage. Consequently, the energy consumption associated with such adjustments is minimized, leading to a more efficient system design for the WSN.

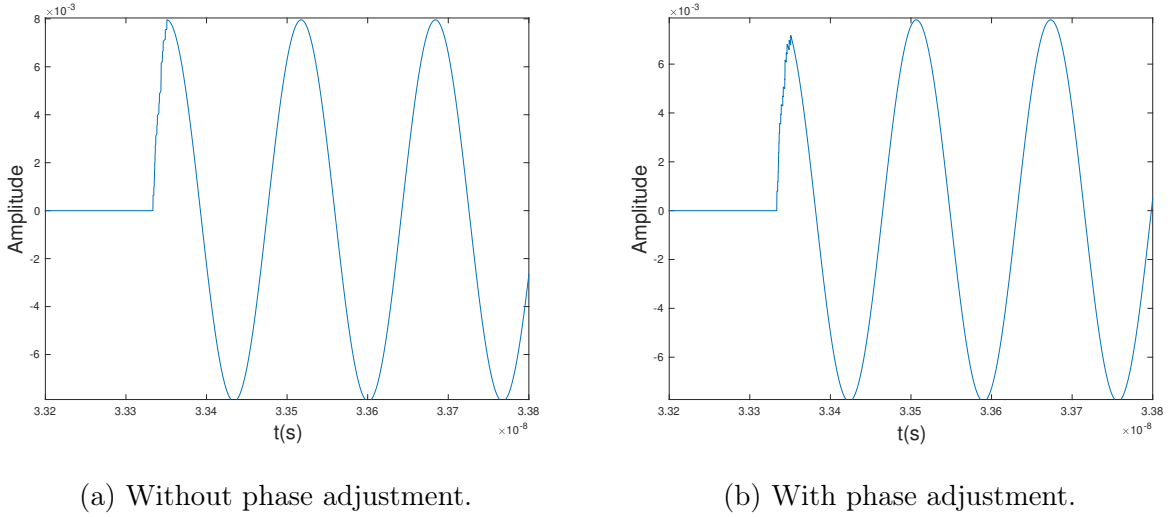


Figure 4.34: Total received signal.

4.10 Multiple groups scenario

To conclude this chapter, we will apply the previously studied concepts to a more complex system comprised of five sensor clusters, each containing 20 individual sensors. These clusters will be integrated into a larger square field measuring 5 meters by 5 meters. Each sensor cluster operates at a frequency of 6GHz and occupies a square area 10λ by 10λ within the field. The drone will be positioned at the center of the entire field, maintaining a height of 10 meters. This configuration ensures the drone remains in the far-field region relative to each cluster while simultaneously experiencing a near-field interaction with the entire sensor network. Fig. 4.35 illustrates the example field used for this analysis.

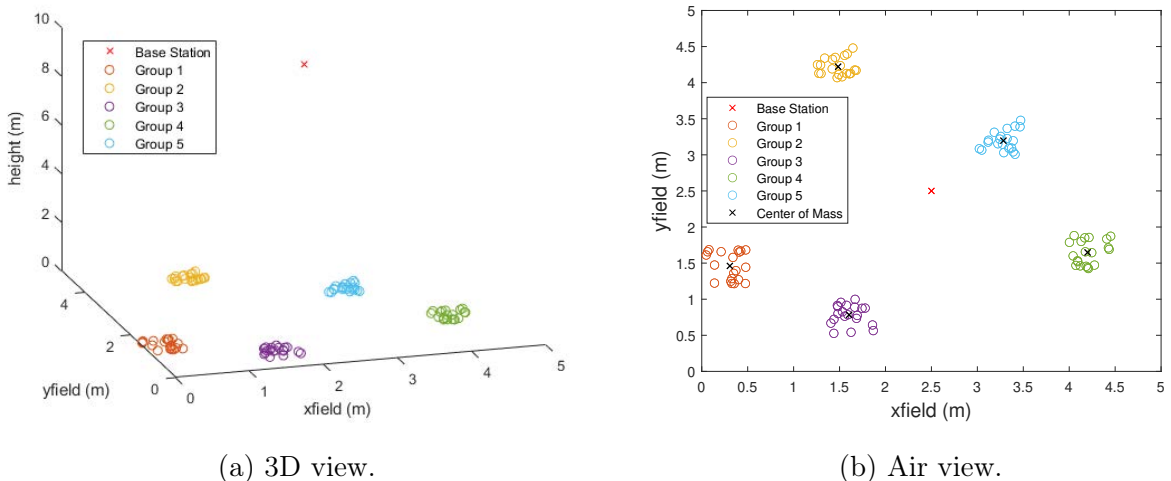


Figure 4.35: Distributed WSN with 5 clusters of sensors randomly placed with drone position error.

As done before, adjustments to every signal were made, obtaining the signals shown in Fig. 4.36.

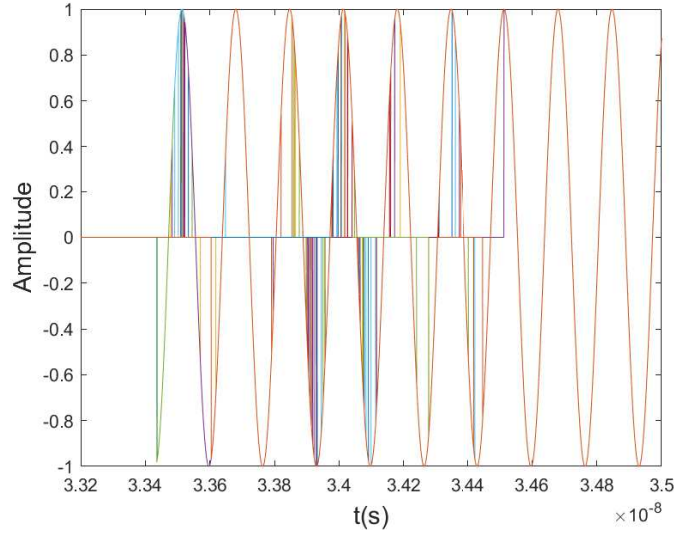


Figure 4.36: Phase-compensated signals at the receiver.

Fig. 4.36 depicts the received signals from the individual sensor clusters. In this scenario, every sensor phase is adjusted individually, maximising the total received signal. As expected, we observe significant time delays in the received signals due to the varying distances between each cluster and the receiver. This highlights the impact of the near-field interaction between the drone and the entire sensor network.

Applying the free-space path loss in each signal, we obtain the received signal shown in Fig. 4.37.

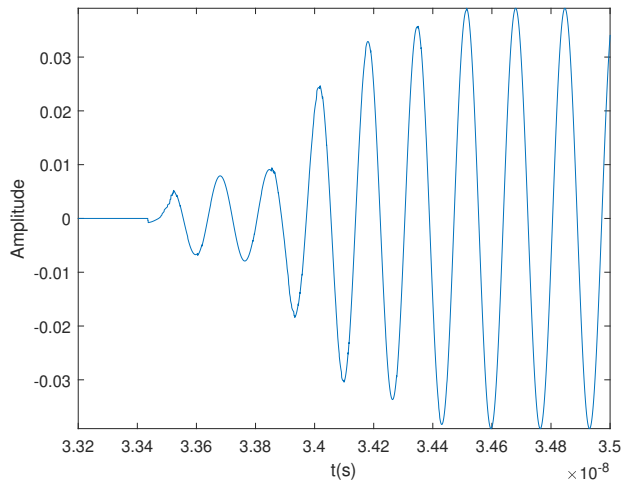


Figure 4.37: Total received signal with phase-compensated approximated to the sensors' exact position.

In contrast to the scenarios observed in previous sections, Fig. 4.37 reveals a key distinction. Here, the signal requires several wave periods to reach a stable state. This extended stabilization period suggests potential challenges in assuming a uniform phase for all sensors within a single cluster.

Fig. 4.16b shows the center of mass for each sensor cluster. In this analysis, we will consider the signal transmitted at the center of mass of each cluster to determine the phase for every sensor within that cluster. This approach aims to evaluate whether the far-field approximation introduced in Section 4.9 can still be applied to this more complex, near-field scenario with multiple sensor clusters.

Thus, applying a phase shift, one for each cluster, results in a catastrophic graph, shown in Fig. 4.38.

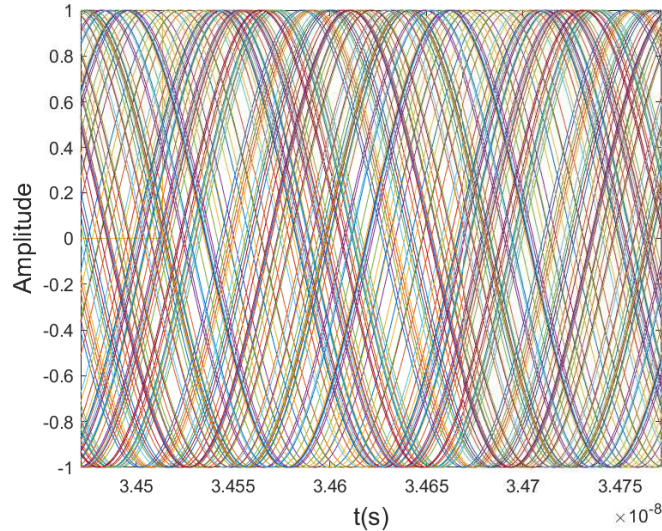


Figure 4.38: Phase-compensated approximated to the center of mass signals at the receiver.

After calculating the phase for each sensor based on the center of mass of its corresponding cluster, we can finally sum the individual signals. The resulting combined signal is shown in Fig. 4.39.

By comparing the received signal when the sensors' phase is approximated to the center of mass, in Fig. 4.39, with the received signal when the sensors' phase is exact to their position, in Fig. 4.37, we can assess the validity and potential error introduced by the approximation technique. This approximation resulted in almost 85% or 16.48dB reduction in the received signal.

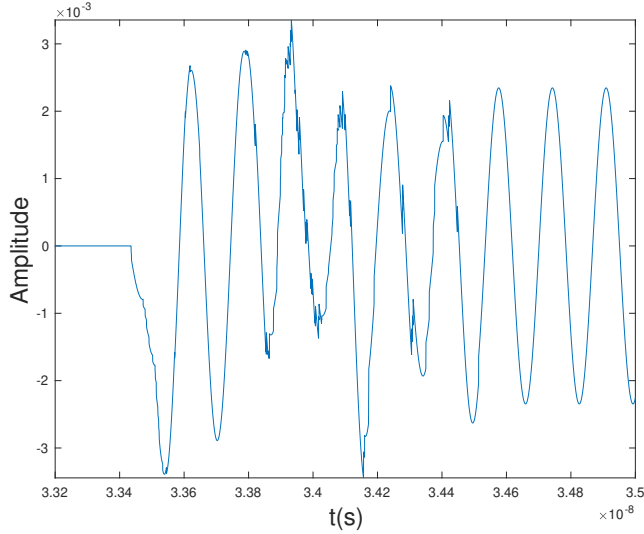


Figure 4.39: Total received signal with phase-compensated approximated to the center of mass.

This reduction can be justified by the height of the drone and the larger distance differences between the sensors and the drone. As exemplified in Fig. 4.40, as the drone moves further away from the center of the group, the worst for the system.

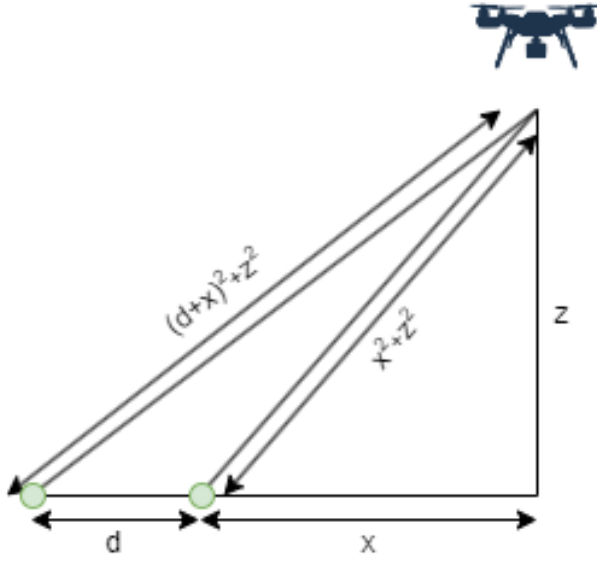


Figure 4.40: Effect of drone moving from the sensor in the far-field approximation.

As demonstrated in the analysis of the multi-cluster system, successfully applying the far-field approximation relies on understanding several key system variables. These include the dimensions of individual sensor clusters, the overall operational area, and the operating frequency. In the scenario presented in Fig. 4.35, one potential solution to ensure far-field

approximations' validity involves reducing the sensor clusters' size. This approach would effectively minimize the distance variations between individual sensors within each cluster and the receiver.

5 Conclusions

This work investigated the performance of WSNs by developing a comprehensive simulation testbed in MATLAB. Studying WSNs in real-world settings is complex, necessitating software simulations. MATLAB provided valuable tools for modelling individual components and processes, particularly those involving multi-dimensional arrays and array factor calculations.

Assuming that the transmitters' and receiver's positions were known, the developed testbed successfully emulated the functionalities of WSNs scenarios. This testbed allowed the understanding of the position errors effect in each WSNs components and their respective influence in scenarios behaviour. A key advantage of the testbed is its configurability. Parameters such as the number of sensors, operating frequency, and sensors and drone's position error variance could be readily adjusted, enabling the analysis of WSN behaviour under various conditions.

Additionally, the study about the position errors in the systems shows that the most crucial point in distributed WSNs is the correct sensor localization due to the great weight in the signal resulting from the communication.

With the results obtained, the importance of beamforming correctly can be observed. This technique, presented throughout the work, allows for the increase of the received power using several sensors in a square space when properly applied. It is also possible to note the difficulties of distributed beamforming compared with conventional beamforming. In conventional beamforming, the sensors' location is practically nonexistent since the space between sensors is the same. In distributed beamforming, the sensors' location is shown to be the most crucial factor. In addition, the inefficient implementation of beamforming can create destructive beamforming, worsening the signal resulting from the system's communication.

In conclusion, this work achieved its primary objective by establishing a versatile testbed for simulating WSNs. The developed platform demonstrates the overall functionality of a WSN system and identifies the sensors' position as the most critical factor for maintaining a

strong received signal. Additionally, the simulations emphasize the importance of localization algorithms with minimal position error variance for achieving robust signal quality in WSNs. These findings pave the way for further research into specific signal propagation effects and developing improved localization algorithms, ultimately contributing to optimising WSN performance.

5.1 Future Work

Having shown that DCBF can enhance WSNs performance, future research can delve deeper into the critical aspects of localization and synchronization for achieving a robust received signal.

An essential area for future research is the evaluation of localization techniques error variance for low-power WSN applications. This evaluation should compare the accuracy, power consumption, scalability, complexity, and cost of various techniques such as Received Signal Strength Indicator (RSSI), Time of Arrival (ToA), Angle of Arrival (AoA), and fingerprinting. By identifying the most suitable techniques that balance accuracy and energy efficiency, we can further enhance the effectiveness of DCBF in WSNs, using this study as base.

Besides existing studies explored open- and closed-loop techniques for synchronization in distributed MIMO systems, several challenges remain. Future research should focus on addressing these challenges, particularly in the areas of:

- **Enhanced synchronization algorithms:** Developing algorithms more robust to clock drift and other synchronization errors.
- **Distributed synchronization protocols:** Designing protocols that enable efficient synchronization across large-scale WSNs.
- **Synchronization with dynamic topologies:** Exploring methods for maintaining synchronization in WSNs with potential changes in network topology.

6 Bibliography

- [1] Ian Akyildiz, Su WY, Y. Sankarasubramaniam, and E. Cayirci. Wireless sensor networks: A survey. *Computer Networks*, 38:393–422, 2002.
- [2] C.A. Balanis. *Antenna Theory: Analysis and Design*. Wiley, 2016.
- [3] J. Benesty, J. Chen, and Y. Huang. Conventional beamforming techniques. In *Microphone Array Signal Processing*, pages 39–65, Berlin, Heidelberg, 2008. Springer Berlin Heidelberg.
- [4] Emil Björnson and Özlem Demir. *Introduction to Multiple Antenna Communications and Reconfigurable Surfaces*. 2024.
- [5] J. Casca. Distributed beamforming. <https://github.com/JoseCasca01/Distributed-Beamforming>, 2024.
- [6] Mauricio Castillo-Effen, D.H. Quintela, Wilfrido Moreno, Ramiro Jordan, and Wayne Westhoff. Wireless sensor networks for flash-flood alerting. pages 142 – 146, 12 2004.
- [7] D. Culler, D. Estrin, and M. Srivastava. Guest editors’ introduction: Overview of sensor networks. *Computer*, 37(8):41–49, 2004.
- [8] H. Fahmy. *Concepts, Applications, Experimentation and Analysis of Wireless Sensor Networks*. 2024.
- [9] Tia Gao, Dan Greenspan, Matt Welsh, Radford Juang, and Alex Alm. Vital signs monitoring and patient tracking over a wireless network. *Conference proceedings : ... Annual International Conference of the IEEE Engineering in Medicine and Biology Society. IEEE Engineering in Medicine and Biology Society. Conference*, 1:102–5, 02 2005.

- [10] Alex B. Gershman, Nicholas D. Sidiropoulos, Shahram Shahbazpanahi, Mats Bengtsson, and Bjorn Ottersten. Convex optimization-based beamforming. *IEEE Signal Processing Magazine*, 27(3):62–75, 2010.
- [11] The MathWorks Inc. Matlab version: 24.1.0.2537033 (r2024a), 2024.
- [12] The MathWorks Inc. Sensor array analyzer: 24.1 (r2024a), 2024.
- [13] The MathWorks Inc. Statistics and machine learning toolbox version: 24.1 (r2024a), 2024.
- [14] Chalermek Intanagonwiwat, Ramesh Govindan, and Deborah Estrin. Directed diffusion: A scalable and robust communication paradigm for sensor networks. *Proceedings of the 6th Annual ACM International Conference on Mobile Computing and Networking.*, 2000.
- [15] Suhanya Jayaprakasam, Sharul Kamal Abdul Rahim, and Chee Yen Leow. Distributed and collaborative beamforming in wireless sensor networks: Classifications, trends, and research directions. *IEEE Communications Surveys & Tutorials*, 19(4):2092–2116, 2017.
- [16] Mohammad Khalaj-Amirhosseini. Synthesis of planar arrays by applying transformations to linear arrays. In *2018 9th International Symposium on Telecommunications (IST)*, pages 39–44, 2018.
- [17] Ala Khalifeh, Khalid Darabkh, Ahmad Khasawneh, Issa Alqaisieh, Mohammad Salameh, Ahmed AlAbdala, Shams Al-Rubaye, Anwar Allassaf, Samer Al-HajAli, Radi Al-Wardat, Novella Bartolini, Giancarlo Bongiovanni, and Kishore Rajendiran. Wireless sensor networks for smart cities: Network design, implementation and performance evaluation. *Electronics*, 10:218, 01 2021.
- [18] Min Lin, Jian Ou-yang, and Jun-Bo Wang. Distributed beamforming for source localization in wireless sensor networks. In *2011 Second International Conference on Mechanic Automation and Control Engineering*, pages 7319–7322, 2011.
- [19] Michael V. Lipski, Sastry Kompella, and Ram M. Narayanan. A pattern shaping approach for distributed collaborative beamforming. In *2023 IEEE Radar Conference (RadarConf23)*, pages 1–6, 2023.
- [20] Thomas L. Marzetta, Erik G. Larsson, Hong Yang, and Hien Quoc Ngo. *Fundamentals of Massive MIMO*. Cambridge University Press, 2016.

- [21] William Merrill. Where is the return on investment in wireless sensor networks? *IEEE Wireless Communications*, 17(1):4–6, 2010.
- [22] Pavel Nikitin, K.V.s Rao, and Steve Lazar. An overview of near field uhf rfid. pages 167 – 174, 04 2007.
- [23] J Quirarte, Norma Ramirez, Jorge Dávalos-Guzmán, and S Ochoa. A novel technique to design phased arrays (scanning).
- [24] Mário Santos and Jaime Santos. Fpga-based control system of an ultrasonic phased array. *Strojniški vestnik – Journal of Mechanical Engineering*, 57, 02 2011.
- [25] Abdulkadir Shallah, Farid Zubir, MKA Rahim, H. Majid, Usman Sheikh, Noor Murad, and Zul Yusoff. Recent developments of butler matrix from components design evolution to system integration for 5g beamforming applications: A survey. *IEEE Access*, PP:1–1, 01 2022.
- [26] Joseph Shaw. Radiometry and the friis transmission equation. *American Journal of Physics*, 81:33–37, 01 2013.
- [27] V. Sneha and M. Nagarajan. Localization in wireless sensor networks: A review. *Cybernetics and Information Technologies*, 20(4):3–26, 2020.
- [28] P. Tait and Institution of Electrical Engineers. *Introduction to Radar Target Recognition*. IEE radar series. Institution of Engineering and Technology, 2005.
- [29] G. Werner-Allen, K. Lorincz, Mario Ruiz, O. Marcillo, J. Johnson, Jonathan Lees, and M. Welsh. Deploying a wireless sensor network on an active volcano. *Internet Computing, IEEE*, 10:18– 25, 04 2006.
- [30] Z. Xiao, L. Zhu, L. Bai, and X. Xia. *Array Beamforming Enabled Wireless Communications*. CRC Press, Taylor & Francis Group, 2023.
- [31] Liang Xue, Jin-Long Wang, Jie Li, Yan-Long Wang, and Xin-Ping Guan. Precoding design for energy efficiency maximization in mimo half-duplex wireless sensor networks with swipt. *Sensors*, 19:4923, 11 2019.
- [32] Jennifer Yick and Dipak Ghosal. Analysis of a prediction-based mobility adaptive tracking algorithm. pages 753 – 760 Vol. 1, 11 2005.